

This is the author's version of the work. It is posted here by permission of the AAAS for personal use, not for redistribution. The definitive version was published in Science , (2021-06-11), doi: 10.1126/science.abg8467. <https://www.science.org/doi/10.1126/science.abg8467>

Title: Release of stem cells from quiescence reveals gliogenic domains in the adult mouse brain

Authors: Ana C. Delgado¹, Angel R. Maldonado-Soto², Violeta Silva-Vargas¹, Dogukan Mizrak^{3,4,10}, Thomas von Känel¹, Kelly R. Tan¹, Alex Paul^{5,9}, Aviv Madar^{7,11}, Henar Cuervo⁸, Jan Kitajewski⁸, Chyuan-Sheng Lin^{3,6} and Fiona Doetsch^{1*}

Affiliations: ¹Biozentrum, University of Basel, Basel, Switzerland, ²Departments of Neurology, ³Pathology and Cell Biology, ⁴Systems Biology, ⁵Genetics and Development, ⁶Herbert Irving Comprehensive Cancer Center, Columbia University Medical Center, ⁷Department of Biology, Center for Genomics and Systems Biology, New York University, ⁸Department of Physiology and Biophysics, University of Illinois at Chicago.

⁹Current Address: Laboratory of Social Evolution and Behavior, Rockefeller University, NYC, USA

¹⁰Current Address: Department of Cardiac Surgery, University of Michigan, Ann Arbor, MI, USA

¹¹Current Address: Valo Health, Boston, MA, USA

*Corresponding author

Fiona Doetsch
Biozentrum, University of Basel
Klingelbergstrasse 50/70
CH 4056 Basel,
Switzerland
Telephone: +41 61 207 22 30
Email: fiona.doetsch@unibas.ch

Abstract: Quiescent neural stem cells (NSCs) in the adult mouse ventricular-subventricular zone (V-SVZ) undergo activation to generate neurons and some glia. Here we show that Platelet-Derived Growth Factor Receptor beta is expressed by adult V-SVZ NSCs that generate olfactory bulb interneurons and glia. Selective deletion of PDGFR β in adult V-SVZ NSCs leads to their release from quiescence uncovering gliogenic domains for different glial cell types. These domains are also recruited upon injury. We identify an intraventricular oligodendrocyte progenitor derived from NSCs inside the brain ventricles that contacts supraependymal axons. Together our findings reveal that the adult V-SVZ contains spatial domains for gliogenesis, in addition to those for neurogenesis. These gliogenic NSC domains tend to be quiescent under homeostasis and may contribute to brain plasticity.

Main Text:

Neural stem cells in the adult mouse ventricular-subventricular zone (V-SVZ) have a regional identity and depending on their spatial location give rise to different subtypes of olfactory bulb interneurons (1). The adult V-SVZ also generates low numbers of glia under baseline conditions, but whether multiple gliogenic domains exist in the V-SVZ is unknown.

The V-SVZ extends along the lateral ventricles, along both the lateral wall, adjacent to the striatum, and the septal wall, adjacent to the septum, which is far less studied (Fig. 1A and Fig. S1D). V-SVZ NSCs are largely quiescent, and both intrinsic and extrinsic signals actively maintain this state. To uncover potential regulators of adult V-SVZ NSC quiescence, we compared the transcriptomes of purified quiescent and activated adult V-SVZ NSCs (2), and identified Platelet-Derived Growth Factor beta (PDGFR β), a tyrosine kinase receptor, as highly enriched in quiescent adult V-SVZ NSCs (qNSCs).

To characterize PDGFR β expression *in vivo* in the V-SVZ, we performed immunostaining with lineage markers. Adult NSCs are radial GFAP⁺ cells (2, 3) that contact the ventricle at the center of pinwheels formed by ependymal cells (4) and have a primary cilium (5). In whole mount preparations, PDGFR β was expressed by NSCs at the center of pinwheels throughout the rostral-caudal extent of the ventricle (Fig. 1B and Fig. S1A, B, E), with their typical radial morphology

revealed by electroporation of a PDGFR β ::mCherry reporter plasmid (Fig. 1C). About 95% of GFAP $^+$ V-SVZ cells expressed PDGFR β (Fig. S1H, L). As NSCs become activated, they upregulate epidermal growth factor receptor (EGFR). PDGFR β was expressed in approximately 50% of activated NSCs (aNSCs, GFAP $^+$ EGFR $^+$, ~2.5% of GFAP $^+$ V-SVZ cells), all of which expressed low levels of EGFR (Fig. 1D and Fig. S1I, M), but not in late aNSCs with high levels of EGFR, transit amplifying cells (TACs, GFAP $^+$ EGFR $^+$) or doublecortin (DCX $^+$) neuroblasts (Fig. 1D and Fig. S1J, K, N). PDGFR β was expressed in CD13 $^+$ pericytes throughout the brain (Fig. S1C, F) and some parenchymal astrocytes (6). We did not detect PDGFR β in Olig2 $^+$ oligodendrocytes (Fig. S1O) or NeuN $^+$ neurons near the V-SVZ. Therefore, within the V-SVZ lineage, PDGFR β is expressed in adult V-SVZ NSCs, which are largely quiescent.

PDGFR β $^+$ V-SVZ cells were long-term neurogenic and gliogenic *in vivo*, as shown by lineage tracing using PDGFR β -P2A-CreER T2 ;mT/mG mice (Fig. S2A). Thirty and 120 days after tamoxifen injection, increasing numbers of GFP $^+$ immature DCX $^+$ and mature NeuN $^+$ neurons were detected in the olfactory bulb, and GFP $^+$ Olig2 $^+$ oligodendrocytes in the corpus callosum (Fig. 1E; and Fig. S2B-F). Within the V-SVZ, GFP $^+$ GFAP $^+$ radial cells, TACs and migrating neuroblasts (Fig. 1F and Fig. S2G-I) were still present at both time points, revealing that PDGFR β $^+$ V-SVZ stem cells generate progeny four months after induction.

To assess the molecular and functional properties of PDGFR β $^+$ NSCs, we FACS purified them from GFAP::GFP mice. The vast majority of GFP $^+$ PDGFR β $^+$ cells were EGFR negative, and corresponded to our previously described CD133 $^+$ and CD133 $^-$ GFP $^+$ populations (P β $^+$ CD133 $^+$) and (P β $^+$) (Fig. 1G) (2). As seen by immunostaining, PDGFR β resolved the EGFR $^+$ aNSCs into two populations, P β $^+$ EGFR $^+$ and P β $^-$ EGFR $^+$ (Fig. 1G). RNA sequencing and functional analysis revealed that expression of PDGFR β was inversely correlated with EGFR expression and cell division (Fig. S2J). The kinetics of colony formation reflected expression of PDGFR β , with P β $^+$ EGFR $^-$ populations having slower kinetics than EGFR $^+$ populations, and the P β $^+$ EGFR $^+$ population in between (Fig. 1H and Fig. S2K). Upon differentiation, all populations were multipotent (Fig. S2L). Genome-wide correlation analysis showed that P β $^+$ EGFR $^+$ cells had correlation scores intermediate between P β $^+$ only and P β $^-$ EGFR $^+$ populations, whereas P β $^+$ only populations were similar to each other and to cortical astrocytes (Fig. 1I). Finally, molecular

comparisons of qNSCs to the $P\beta^+EGFR^+$ population highlighted known (2, 7) and novel GO quiescence pathways (Fig. S2M, Tables S1-3). In contrast, pathways including those related to entry into cell cycle and regulation of translation initiation were enriched in $P\beta^+EGFR^+$ cells (Fig. S2N). Consistent with their faster *in vitro* activation kinetics, the majority of pathways enriched in $P\beta^+EGFR^+$ versus $P\beta^+EGFR^+$ cells were cell-cycle and cytoskeletal remodeling related (Fig. S2O, P).

To functionally assess the effect of deleting $PDGFR\beta$ selectively in adult $GFAP^+$ V-SVZ NSCs *in vivo*, we generated inducible triple transgenic $hGFAP::CreER^{T2};PDGFR\beta^{+/+};A14$ ($PDGFR\beta^{WT}$) and mutant $hGFAP::CreER^{T2};PDGFR\beta^{fl/fl};A14$ ($PDGFR\beta^{\Delta}$) mice in which $CreER^{T2}$ recombinase is under the control of the human GFAP promoter ($hGFAP::CreER^{T2}$). Upon tamoxifen injection, the first and second immunoglobulin domains of the *pdgfrb* gene are deleted preventing PDGF-ligand binding (8) and tdTomato is expressed allowing cell fate to be followed (Fig. S3A). Phosphorylation of $PDGFR\beta$ was greatly reduced in Tom^+ radial stem cells in $PDGFR\beta^{\Delta}$ mice (Fig. S3B). Deletion of $PDGFR\beta$ led to an increase in activated stem cells and dividing stem cells one day after ending tamoxifen injections (1dpi) (Fig. 2A-D). TACs and neuroblasts were also increased (Fig. 2A and Fig. S3C-D). We also detected a small increase in $Tom^+Caspase3^+$ cells in $PDGFR\beta^{\Delta}$ mice, consistent with a role for $PDGFR\beta$ in cell survival in other cell types (9) (Fig. S3E-F), but their proportion was very low compared to the large increase in total Tom^+ cell number. The increased activation of NSCs in $PDGFR\beta^{\Delta}$ mice resulted in more mature neurons in the olfactory bulb (Fig. 2E, F) and more oligodendrocytes in the corpus callosum than in control mice at 45 and 180 dpi (Fig. 2G, H). Stem cell activation and progeny remained increased at later timepoints in the V-SVZ (Fig. S3G-I).

Adult NSCs contact the ventricle and are bathed by cerebrospinal fluid. PDGFDD ligand, which binds specifically to $PDGFR\beta$, was detected by ELISA in both the cerebrospinal fluid and the choroid plexus, a key source of secreted factors in the cerebrospinal fluid (10) (Fig. S3J). To independently confirm that blocking $PDGFR\beta$ signaling promotes qNSC activation, we cultured FACS purified qNSCs with PDGFDD ligand and $PDGFR\beta$ blocking antibodies. Again, more qNSCs became activated to give rise to colonies, and with faster activation kinetics, than with isotype controls (Fig. 2I, J).

PDGFR β is therefore expressed in qNSCs in the adult V-SVZ, and is down-regulated as stem cells activate. Indeed, deletion of PDGFR β selectively in adult NSCs releases them from quiescence, in contrast to deleting PDGFR β embryonically (11, 12). As such, PDGFR β likely exerts distinct functions at different stages of brain development and in different cell types, such as pericytes (13, 14).

The release of adult NSCs from quiescence in PDGFR β^{Δ} mice provides a powerful tool to uncover V-SVZ NSC domains *in vivo* that are normally more quiescent. In the adult V-SVZ, olfactory bulb interneurons arise from throughout the lateral wall and rostral levels of the septal wall, and oligodendrocytes from the dorsal-lateral V-SVZ (1, 15). PDGFR β^{Δ} mice revealed both unknown glial cell types and several gliogenic domains in the adult V-SVZ, which are less proliferative under homeostasis.

Several types of GFAP $^{+}$ cells with different distributions and morphologies in the V-SVZ were present in both wild type and PDGFR β^{Δ} mice. Radial GFAP $^{+}$ cells with a process perpendicular to the ventricle were present in both lateral and septal walls, but were more enriched in the dorsal and ventral V-SVZ (Fig. 3A, B and Fig. S4A). A second radial GFAP $^{+}$ cell with a process parallel to the ventricle was more prevalent on the septal side (Fig. 3A, B and Fig. S4B). At 1dpi, both were significantly increased (Fig. 3C).

We identified an astrocytic cell type, which we named gorditas, with a rounded soma with short GFAP $^{+}$ processes (Fig. 3A, B and Fig. S4C), enriched in the septal side and rare in wild type mice. In contrast to mature stellate parenchymal astrocytes, which express low levels of GFAP (Fig. S4D) and have a highly branched and bushy morphology, gorditas were strongly GFAP $^{+}$, had smaller soma and nuclei (Fig. S4E, F, H) and fewer primary processes (Fig. S4G, H, K). About 70% expressed dim nestin (Fig. S4I) and they were rarely MCM2 $^{+}$ in either control or PDGFR β^{Δ} mice. Gorditas were most prevalent adjacent to the mid-ventral septal wall from rostral to mid levels (Bregma +1.25 to +0.5mm) of the V-SVZ (Fig. S4J, L, M), and were significantly increased only in this septal domain of PDGFR β^{Δ} mice (Fig. 3C and Fig. S4J), at both 1dpi and 45dpi (Fig. 3D). Tom $^{+}$ mature stellate astrocytes were also increased in the septum (Fig. S4M, N), but not in the striatum or cortex (Fig. S4O) at 45dpi in PDGFR β^{Δ} mice. Together,

these highlight the diversity of astrocytes in the septal region.

The release from quiescence also uncovered multiple oligodendrogenic domains. We mapped their distribution by quantifying Tom⁺Olig2⁺ cells in different subregions of the V-SVZ at 1dpi (Fig. 3E and Fig. S5A-F). The dorsolateral wedge, known to be oligodendrogenic (15), and corpus callosum had increased Tom⁺Olig2⁺ cells in PDGFRβ^{-/-} mice (Fig. S5A, B). Overall, the septal wall contained more Tom⁺Olig2⁺MCM2⁺ cells than the lateral wall (Fig. 3G and Fig. S5F, G), with a focal hot spot in the dorso-septal corner (Fig. 3F, G and Fig. S5F, H). These septal Olig2⁺ domains were already present during development at postnatal days 1 and 10 (Fig. S5 I, J). In addition to the dorsolateral wedge, another oligodendrogenic domain was present in the lateral wall at more caudal levels (Fig. S5F). Our single cell transcriptional profiling indicated that the septal wall is more oligodendrogenic than the lateral wall (16). We therefore compared the differentiation potential of FACS-purified PDGFRβ⁺GFAP⁺:GFP⁺ adult NSCs from both walls of adult wild type mice, which directly showed that septal NSCs gave rise to more O4⁺ oligodendrocytes and fewer TuJ1⁺ neurons than lateral NSCs (Fig. S5K, L).

The above gliogenic domains are largely quiescent under homeostasis. To investigate whether they respond to injury in wild type mice we performed focal demyelination in the corpus callosum by unilateral injection of lysolecithin (Fig. S6A, B). At 2dpi, dividing MCM2⁺ cells increased around the ipsilateral ventricle (Fig. S6C). More radial stem cells were recruited to divide in both the septal and lateral walls (Fig. S6D-F). Olig2⁺MCM2⁺ cells were increased in all domains at 2dpi (Fig. 3H, I and Fig. S6J), but became restricted to septal domains at 5dpi (Fig. S6K, L). Gorditas were also increased in lysolecithin injected mice, and many were MCM2⁺ (Fig. 3J, K and Fig. S6G-I). Thus, these more quiescent gliogenic domains, as well as gorditas, are recruited in response to physiological demand.

Unexpectedly, we also identified an unknown PDGFRα⁺ cell type inside the brain ventricles, which we call intraventricular oligodendrocyte progenitors (OPCs). In PDGFRβ^{-/-} mice, numerous intraventricular Tom⁺Olig2⁺ cells derived from GFAP⁺ NSCs were attached to the luminal surface of the wall (Fig. 4A). Intraventricular OPCs were also present in wild type brains, which we characterized further. Their morphology and distribution were most clearly visualized in

whole mount preparations. Intraventricular OPCs were localized on top of ependymal cells nestled between their cilia (Fig. 4B, C), in the rostral portion of both the lateral and septal walls of the ventricle (Fig. S7A, B, E). They expressed typical OPC markers (Olig2⁺, NG2⁺ and PDGFR α ⁺) (Fig. 4B-D and Fig. S7F) and frequently contacted each other (Fig. S7A, B). Lineage tracing and immunostaining showed that intraventricular OPCs arose from tight clusters of GFAP⁺PDGFR β ⁺ cells (Fig. 4D), which gave rise to PDGFR α ⁺ cells, some of which retained GFAP, that then dispersed as individual PDGFR α ⁺ only cells, with an increasingly ramified morphology (Fig. S7C, G, H, J). Intraventricular OPCs differed morphologically from PDGFR α ⁺ OPCs found in the SVZ and brain parenchyma (Fig. 4B and Fig. S7C, D). Unlike parenchymal OPCs, they expressed EGFR in the nucleus, and many were Ascl1⁺ (Fig. S7K, L). Some were dividing based on MCM2 and Ki67 expression (Fig. S7M-O). Intraventricular OPCs first appeared around postnatal day 5 and 7 (Fig. S8A), paralleling an increase in PDGFAA ligand in the choroid plexus (Fig. S8B), and increased in number to two months. Their number decreased over time and at 14 months clusters were still present, but few dispersed cells (Fig. S8A). After focal demyelination with LPC, intraventricular OPCs initially disappeared at 2dpi, but then increased in number at 5dpi (Fig. S8C-G).

Many intraventricular OPCs were closely apposed to or partially enwrapped supraependymal axons present on the surface of the both walls of the lateral ventricles, including serotonergic axons (Fig. 4E, F, and Fig. S8H) that regulate NSC proliferation (17). We did not detect mature myelinating Rip, MOG or MBP⁺ oligodendrocytes inside the ventricles (Fig. S7P-R), suggesting that intraventricular OPCs do not give rise to myelinating oligodendrocytes *in situ*. Given their location, intraventricular OPCs are poised to integrate and dynamically respond to signals from the cerebrospinal fluid and diverse cell types, including axons from other brain regions.

Here, we uncover multiple gliogenic domains in the adult V-SVZ that are more quiescent under homeostasis and are recruited in response to focal injury. Stem cells in these spatially distinct domains may be differentially recruited in different physiological states, as occurs for olfactory bulb neuron subtypes (18), to generate specific glial subtypes in a context-dependent manner. The identification of two unknown glial cell types in the adult brain further highlights the extent of glial diversity and opens vistas into understanding the role of neural stem cells and glia in

health and disease.

References

1. Z. Chaker, P. Codega, F. Doetsch, A mosaic world: puzzles revealed by adult neural stem cell heterogeneity. *Wiley Interdiscip Rev Dev Biol* 5, 640-658 (2016).
2. P. Codega et al., Prospective identification and purification of quiescent adult neural stem cells from their in vivo niche. *Neuron* 82, 545-559 (2014).
3. F. Doetsch, I. Caille, D. A. Lim, J. M. Garcia-Verdugo, A. Alvarez-Buylla, Subventricular zone astrocytes are neural stem cells in the adult mammalian brain. *Cell* 97, 703-716 (1999).
4. Z. Mirzadeh, F. T. Merkle, M. Soriano-Navarro, J. M. Garcia-Verdugo, A. Alvarez-Buylla, Neural stem cells confer unique pinwheel architecture to the ventricular surface in neurogenic regions of the adult brain. *Cell Stem Cell* 3, 265-278 (2008).
5. F. Doetsch, J. M. Garcia-Verdugo, A. Alvarez-Buylla, Regeneration of a germinal layer in the adult mammalian brain. *Proc Natl Acad Sci U S A* 96, 11619-11624 (1999).
6. M. Vanlandewijck et al., A molecular atlas of cell types and zonation in the brain vasculature. *Nature* 554, 475-480 (2018).
7. E. Llorens-Bobadilla et al., Single-Cell Transcriptomics Reveals a Population of Dormant Neural Stem Cells that Become Activated upon Brain Injury. *Cell Stem Cell* 17, 329-340 (2015).
8. J. Schmahl, K. Rizzolo, P. Soriano, The PDGF signaling pathway controls multiple steroid-producing lineages. *Genes Dev* 22, 3255-3267 (2008).
9. Y. Ishii et al., Mouse brains deficient in neuronal PDGF receptor-beta develop normally but are vulnerable to injury. *J Neurochem* 98, 588-600 (2006).
10. V. Silva-Vargas, A. R. Maldonado-Soto, D. Mizrak, P. Codega, F. Doetsch, Age-Dependent Niche Signals from the Choroid Plexus Regulate Adult Neural Stem Cells. *Cell Stem Cell* 19, 643-652 (2016).
11. Y. Ishii et al., Characterization of neuroprogenitor cells expressing the PDGF beta-receptor within the subventricular zone of postnatal mice. *Mol Cell Neurosci* 37, 507-518 (2008).
12. G. Xu et al., Functional analysis of platelet-derived growth factor receptor-beta in neural stem/progenitor cells. *Neuroscience* 238, 195-208 (2013).
13. A. Armulik et al., Pericytes regulate the blood-brain barrier. *Nature* 468, 557-561 (2010).
14. R. Daneman, L. Zhou, A. A. Kebede, B. A. Barres, Pericytes are required for blood-brain barrier integrity during embryogenesis. *Nature* 468, 562-566 (2010).
15. K. Azim, B. Berninger, O. Raineteau, Mosaic Subventricular Origins of Forebrain Oligodendrogenesis. *Front Neurosci* 10, 107 (2016).
16. D. Mizrak et al., Single-Cell Analysis of Regional Differences in Adult V-SVZ Neural Stem Cell Lineages. *Cell Rep* 26, 394-406 e395 (2019).
17. C. K. Tong et al., Axonal control of the adult neural stem cell niche. *Cell Stem Cell* 14, 500-511 (2014).
18. A. Paul, Z. Chaker, F. Doetsch, Hypothalamic regulation of regionally distinct adult neural stem cells and neurogenesis. *Science* 356, 1383-1386 (2017).
19. H. Cuervo et al., PDGFRbeta-P2A-CreER(T2) mice: a genetic tool to target pericytes in angiogenesis. *Angiogenesis* 20, 655-662 (2017).

20. L. Zhuo et al., Live astrocytes visualized by green fluorescent protein in transgenic mice. *Dev Biol* 187, 36-42 (1997).
21. Y. M. Ganat et al., Early postnatal astroglial cells produce multilineage precursors and neural stem cells in vivo. *J Neurosci* 26, 8609-8621 (2006).
22. A. E. Ballagi, A. Ishizaki, J. O. Nehlin, K. Funa, Isolation and characterization of the mouse PDGF beta-receptor promoter. *Biochem Biophys Res Commun* 210, 165-173 (1995).
23. F. Barnabe-Heider et al., Genetic manipulation of adult mouse neurogenic niches by in vivo electroporation. *Nat Methods* 5, 189-196 (2008).
24. F. Doetsch, A. Alvarez-Buylla, Network of tangential pathways for neuronal migration in adult mammalian brain. *Proc Natl Acad Sci U S A* 93, 14895-14900 (1996).
25. Z. Mirzadeh, F. Doetsch, K. Sawamoto, H. Wichterle, A. Alvarez-Buylla, The subventricular zone en-face: wholemount staining and ependymal flow. *J Vis Exp*, (2010).
26. J. Schindelin et al., Fiji: an open-source platform for biological-image analysis. *Nat Methods* 9, 676-682 (2012).
27. C. Trapnell et al., Transcript assembly and quantification by RNA-Seq reveals unannotated transcripts and isoform switching during cell differentiation. *Nat Biotechnol* 28, 511-515 (2010).
28. M. Martin, Cutadapt removes adapter sequences from high-throughput sequencing reads. *EMBnet.journal*, [S.l.], v. 17, n. 1, p. pp. 10-12, 17, 2 (2011).
29. S. Anders, P. T. Pyl, W. Huber, HTSeq--a Python framework to work with high-throughput sequencing data. *Bioinformatics* 31, 166-169 (2015).
30. M. D. Robinson, D. J. McCarthy, G. K. Smyth, edgeR: a Bioconductor package for differential expression analysis of digital gene expression data. *Bioinformatics* 26, 139-140 (2010).

Acknowledgements

We thank members of the Doetsch and Wichterle labs and D. Thaler for discussion; V. Crotet for genotyping; the Biozentrum Imaging Core Facility; K. Gordon and S. Tetteh of the Herbert Irving Comprehensive Cancer Center Flow Cytometry Core of Columbia University for assistance with FACS; and J. Bögli at the Biozentrum FACS Core Facility. **Funding:** This work was supported by NIH NINDS R01 NS074039 (F.D), Swiss National Science Foundation 31003A_163088 (F.D), European Research Council Advanced Grant (No 789328) (FD) and the University of Basel, NINDS grant 1F31NS079057 (A.R.M-S.), NRSA Ruth Kirschstein Postdoctoral Fellowship NINDS F32 NS090736 (D.M), Swiss National Science Foundation BSSGIO_155830 (K.R.T), NINDS F31NS089252 (A.P), NIH NHLBI R01 HL112626 (J.K.) and NCI 5P30CA013696 (C-S.L). **Author Contributions:** Conceptualization: F.D., A.R.M-S., A.C.D.; Performed experiments: A.C.D., A.R.M-S., V.S-V., D.M., T.vK., K.R.T, A.P., H.C.;

Data Analysis: A.C.D., A.R.M-S., V.S-V., D.M., A.M.; Supervision: F.D.; Manuscript writing: A.C.D., A.R.M-S., V.S-V. , D.M. and F.D.; Resources: H.C., J.K. and C-S.L contributed PDGFR β -P2A-CreER^{T2};mT/mG mice. **Competing Interests:** The authors declare no competing interests. **Data and materials availability:** All data are deposited in the National Center for Biotechnology Information Gene Expression Omnibus under accession number GSE118009.

Supplementary Materials

Materials and Methods

Figures S1-S8

Tables S1-S3

References (19-30)

Fig. 1 PDGFR β is expressed by adult V-SVZ NSCs

(A) Schema of whole mouse brain (top) and coronal section (bottom) at level of dashed line. The V-SVZ is adjacent to the lateral ventricles (V, green) and generates neurons that migrate to the olfactory bulb (OB). (B) Whole mounts showing clusters of PDGFR β ⁺ NSCs (green) at center of ependymal cell pinwheels (dashed line shows one pinwheel). (C) Radial morphology of PDGFR β ::mCherry electroporated cell. Color code indicates depth relative to ventricular surface. (D) Coronal sections showing PDGFR β immunostaining in quiescent (orange arrowhead) and some activated (white arrowhead) NSCs, but not in TACs (asterisks). (E, F) Lineage-tracing of PDGFR β ⁺ cells showing GFP⁺ new neurons in the OB (E) and radial stem cells in V-SVZ (F) (arrowheads) at 120dpi. (G) Representative FACS multigraph overlay showing distribution of PDGFR β ⁺ cells in purified GFAP β ::GFP⁺CD24⁻ subpopulations gated on EGFR and CD133. (H) Activation kinetics of FACS purified populations *in vitro*; n=5. (I) Genome-wide correlation analysis of gene expression profiles. V, ventricle; *Str*, striatum; *Sp*, septum; Scale bars, 10 μ m.

Fig. 2 PDGFR β deletion releases adult NSCs from quiescence

(A) Quantification of Tom⁺ aNSCs, TACs and (B) GFAP⁺ dividing cells at 1dpi PDGFR β ^{WT} and PDGFR β ^{-/-} mice; n=4. (C) Immunostaining of V-SVZ coronal sections showing Tom⁺ aNSCs and (D) dividing GFAP⁺ cells at 1dpi (arrowheads). (E) Images of Tom⁺NeuN⁺ neurons in the olfactory bulb (OB) and (F) quantification at 45 and 180 dpi; n=4. (G) Tom⁺Olig2⁺ cells (arrowheads) in the corpus callosum (cc) and quantification (H) at 45 and 180dpi; n=4. (I) Time course of activation and (J) images of P β ⁺CD133⁺ qNSCs treated with PDGFDD or PDGFDD + α PDGFR β ; n=5. *Str*, striatum; *Sp*, septum. Scale bars, 10 μ m. *p<0.05, ***p<0.001. Error bars indicate SEM.

Fig. 3 Gliogenic domains in the adult V-SVZ

(A) Coronal schema depicting distribution of different types of GFAP⁺ cells in adult V-SVZ. Boxes and numbers show location of images in B. (B) Different types of Tom⁺GFAP⁺ cells (arrowheads) at 1dpi. (C) Quantification of radial cells and gorditas in the lateral and septal walls at 1dpi; n=4. (D) Quantification of gorditas in septal wall at 45 dpi; n=4. (E-G) Oligodendrogenic domains. (E) Coronal schema showing domains analyzed in the V-SVZ. (F) Tom⁺Olig2⁺ cells (arrowhead) in dorsal-septal corner of V-SVZ. (G) Quantification of Tom⁺Olig2⁺ cells in different domains of V-SVZ from Bregma +1.2mm to 0mm in PDGFRβ^{WT} and PDGFRβ^Δ mice; n=4. (H-K) Demyelination. (H) Images of Olig2⁺MCM2⁺ cells (arrowheads) and (I) quantification in different V-SVZ domains at 2dpi; n=3. (J) Images of gorditas (arrowheads) in septal wall at 2dpi and (K) their quantification at 2 and 5dpi; n=3. *Str*, striatum; *Sp*, septum; V, ventricle, LPC, lysolecithin. Scale bars, B, F, H, J, 10μm. *p<0.05, **p<0.01, ***p<0.001. #p<0.05, ##p<0.01 (MCM2 comparisons). Error bars indicate SEM.

Fig. 4 Intraventricular oligodendrocyte progenitors

(A) Tom⁺Olig2⁺ intraventricular OPCs in coronal sections of PDGFRβ^{WT} and PDGFRβ^{-/-} mice. (B-F) Whole mount immunostaining of intraventricular OPCs in wild type mice. (B) PDGFRα⁺ OPCs on ventricular surface (β-catenin) and (C) among the cilia of ependymal cells (ac-tubulin). (D) PDGFRβ⁺GFAP⁺NG2⁺ cluster (white arrowhead) and dispersed NG2⁺ OPCs that are PDGFRβ⁻ (blue arrowhead). (E-F) Association of intraventricular OPCs with supraependymal Neurofilament⁺ (E) and serotonergic (5-HT) (F) axons. Scale bars, 10μm.

Figure 1

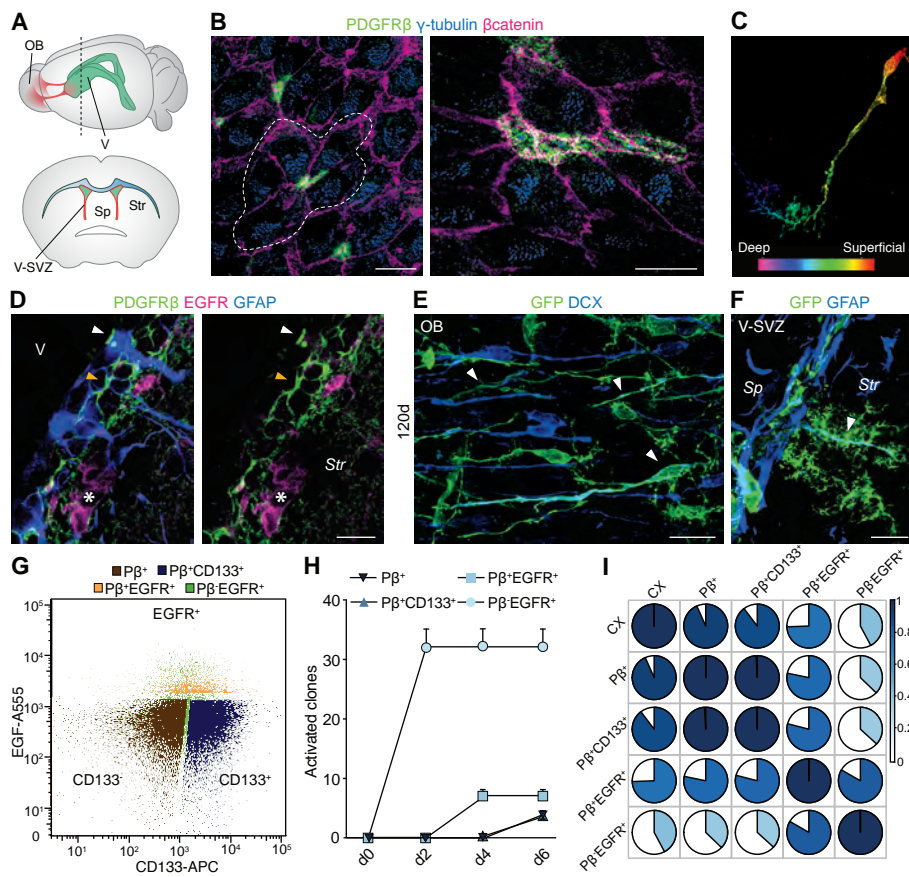


Figure 2

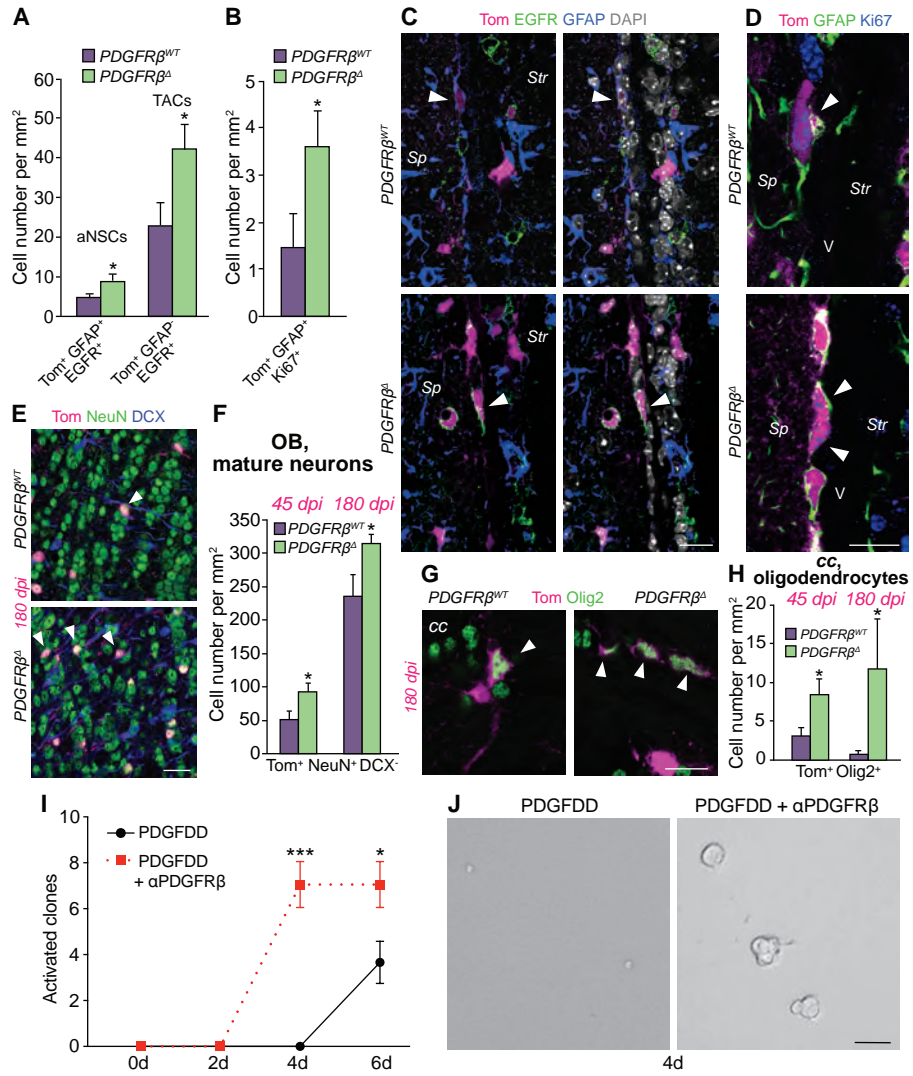


Figure 3

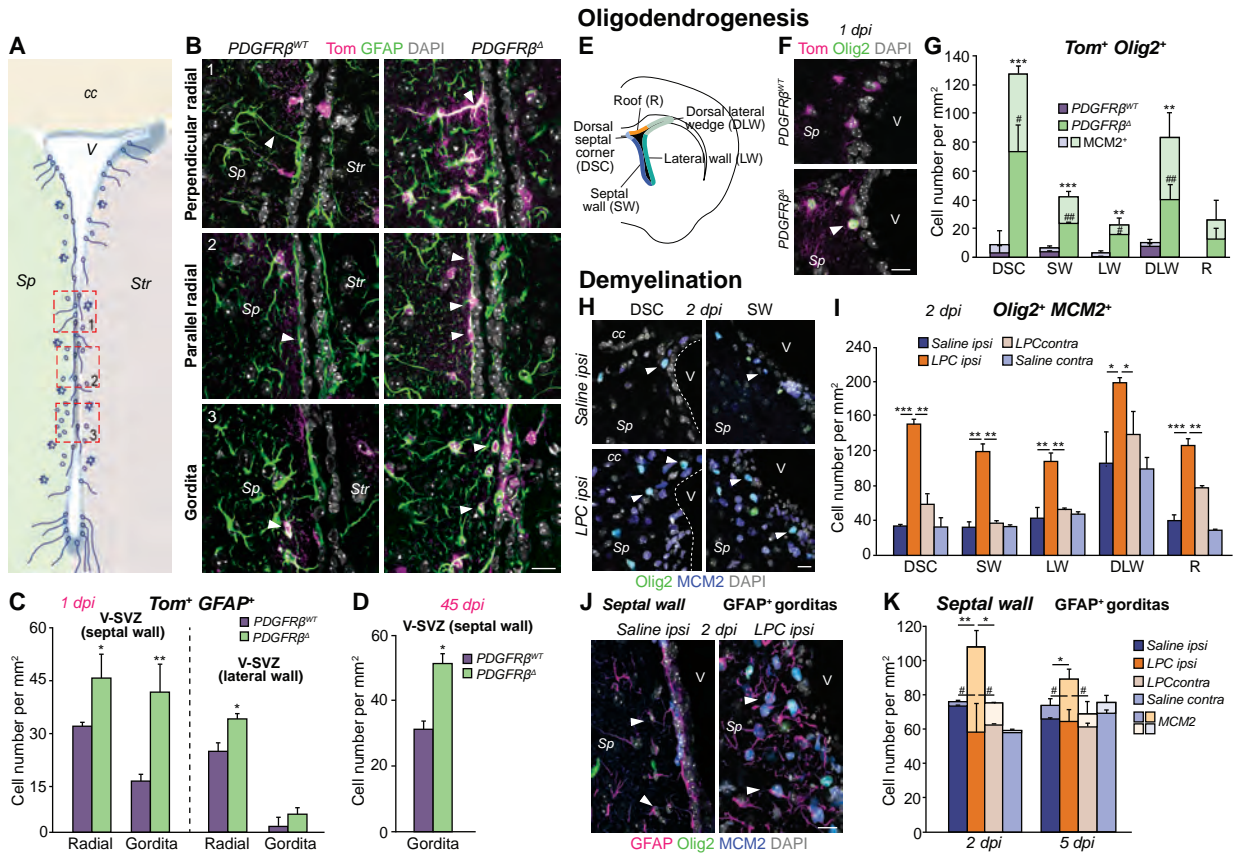
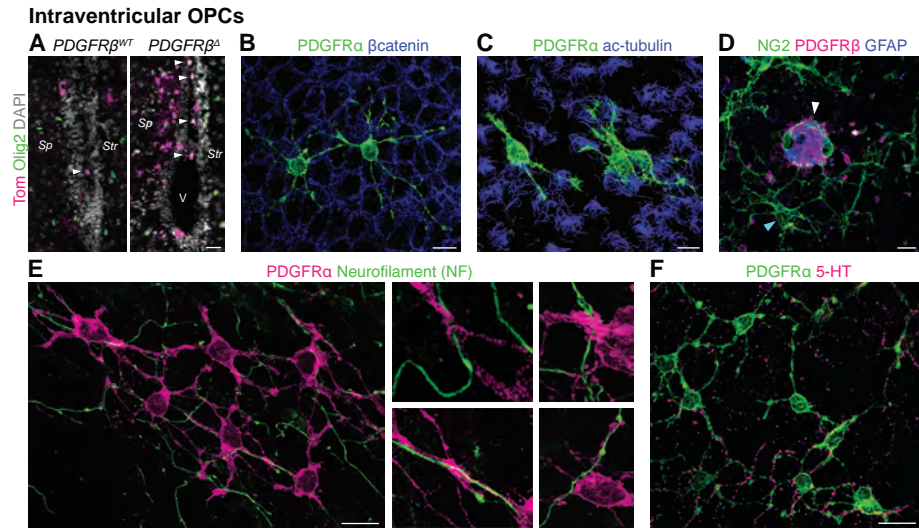


Figure 4



Supplementary Materials for

Release of stem cells from quiescence reveals gliogenic domains in the adult mouse brain

Ana C. Delgado, Angel R. Maldonado-Soto, Violeta Silva-Vargas, Dogukan Mizrak, Thomas von Känel, Kelly R. Tan, Alex Paul, Aviv Madar, Henar Cuervo, Jan Kitajewski, Chyuan-Sheng Lin and Fiona Doetsch

Correspondence to: fiona.doetsch@unibas.ch

This PDF file includes:

Materials and Methods
Figs. S1 to S8
Captions for Tables S1 to S3

Other Supplementary Materials for this manuscript include the following:

Table S1. RNA seq. List of expression values in FPKM (fragments per kilobase of transcript per million mapped reads) from 5 FACS purified populations

Table S2. RNA seq. List of differentially expressed genes across PDGFR β^+ qNSCs, PDGFR β^+ EGFR $^+$ and PDGFR β^- EGFR $^+$ population comparisons.

Table S3. Top enriched pathway maps from Metacore analysis comparing PDGFR β^+ qNSCs, PDGFR β^+ EGFR $^+$ and PDGFR β^- EGFR $^+$ populations.

Materials and Methods

Animals

All adult mice used were two to three months old, with the exception of 6, 9 and 14 month old mice used for intraventricular OPC characterization. The following mouse lines were used: CD1 (Charles River), RjOrl:SWISS (Janvier), C57BL/6JRj (Janvier), PDGFR β -P2A-CreER^{T2};mT/mG mice (19) (generated and provided by H. Cuervo, J. Kitajewski and C-S. Lin; PDGFR β -P2A-CreER^{T2} now available from Jackson Laboratory Stock No. 030201)), hGFAP::GFP mice (20) (Jackson Laboratory Stock No. 003257). We bred hGFAP::CreER^{T2} (Jackson Laboratory Stock No. 012849) (21), PDGFR β ^{fl/+} (Jackson Laboratory Stock No. 010977) (8), and Gt(ROSA)26Sor^{tm14(CAG-tdTomato)Hze} (Ai14; Jackson Laboratory Stock No. 007914) mice together to generate triple transgenic mice hGFAP::CreER^{T2};PDGFR β ^{fl/fl};A14 (PDGFR β^{Δ}) or hGFAP::CreER^{T2};PDGFR β ^{+/+};A14 (PDGFR β^{WT}). We used males for the deletion experiments, and both males and females for characterization of intraventricular OPCs, lineage tracing experiments and postnatal analysis (P1-P15).

Experiments were performed in accordance with Columbia University IACUC guidelines and approval of the cantonal veterinary office of Basel-Stadt (license numbers 2859 and 2742).

Tamoxifen administration

Cre-mediated recombination in CreER^{T2} transgenic mice was induced by administration of Tamoxifen (Sigma) dissolved at 30 mg/ml in corn oil (Sigma). Mice were injected intraperitoneally (120mg/kg) once per day for 3 consecutive days and sacrificed at different points after ending tamoxifen injections: For lineage tracing, mice were analyzed 7, 30 and 120

days post injection (dpi). For PDGFR β deletion experiments, mice were sacrificed 1 dpi, 45 dpi or 180 dpi.

Cloning

The PDGFR β promoter was cloned from mouse genomic DNA using the following primers:

AseIF 5'-GCCATTAATGCTGGGTCAGGCACTCC-3' and *XhoIR* 5'-

ATACTCGAGCTCCGGGAGGAGCGGAGCA-3'. The region amplified by these primers

contained a CCAAT motif in the promoter necessary to drive a luciferase assay (22). In order to

insert the promoter into the CherryPicker (Clontech) membrane-bound mCherry expression

vector we performed site-directed mutagenesis to remove an AgeI site from the promoter. We

used the QuickChange Site- Directed Mutagenesis kit (Stratagene) and the following primers:

sdmF 5'-GCACACAGTACCGGCCCTCAGGTCCTCAAAC-3' *sdmR* 5'-

GTTTGAGGACCTGAGGGCCGGTACTGTGTGC-3'. The promoter with the point mutation was

inserted into the CherryPicker vector using *XhoI* and *AgeI* restriction sites and the following

primers: *XhoIF* 5'-CACCTCGAGACCGCTGGGTCAGGCACTCC-3' *AgeIR* 5'-

ATAACCGGTCTCCGGGAGGAGCGGAGCA-3'.

Electroporation

The electroporation protocol was adapted from (23). CD1 mice were deeply anesthetized using

Avertin (Sigma). 1 μ l of solution containing 5 mg/ml of PDGFR β ::mCherry plasmid in 0.9%

saline was injected into the lateral ventricle using the following coordinates relative to Bregma:

anterior-posterior, 0.0; lateral, 0.85; ventral, -2.5 mm. Holding the cathode of a square

electroporator towards the ipsilateral V-SVZ, five pulses of 200 V (50 ms; separated by 950 ms)

were administered and mice sacrificed 7 days later.

Tissue preparation for Immunohistochemistry

Mice were anesthetized by intraperitoneal injection with pentobarbital or Avertin and were sacrificed by intracardial perfusion of 4% paraformaldehyde (PFA) in 0.1M phosphate buffer (PB). Brains were extracted from the skull and post-fixed 3 hours for immunostaining for receptors and overnight for all other antibodies. Coronal sections were cut at 25 μ m using a vibrating microtome (Leica VT1000S). Whole mounts were prepared as previously described (24, 25).

In vivo immunostaining

Brain sections and whole mount preparations were incubated in blocking solution (PBS with 3% bovine serum albumin (BSA) and 0.5% Triton-X100 for sections or 1.5% Triton-X100 for whole mounts) for 60 minutes and then incubated in primary antibodies in blocking solution for 36 hours at 4°C. After washing, sections and whole mounts were incubated with secondary antibodies for 1-2 hours at room temperature, washed, counterstained with 4',6- Diamidino-2-Phenylindole Dihydrochloride (DAPI, Sigma) and mounted on slides with FluorSave™ (Millipore Corporation).

Antibodies

The following primary antibodies were used: anti-adenylate cyclase (rabbit, 1:100, Santa Cruz Biotechnology, Cat# sc-588, discontinued); anti-CD13 (rat, 1:100, abcam, Cat# ab33489, RRID: AB_726095); anti-cleaved caspase 3 (rabbit, 1:100, Cell Signaling, Cat# 9661, RRID: AB_2341188); anti- β -Catenin (mouse, 1:200, BD Bioscience, Cat# 610153, RRID: AB_397554); anti- β -Catenin (rabbit, 1:200, Cell signaling, Cat# 9587, RRID: AB_10695312); anti-doublecortin, DCX (goat, 1:100, Santa Cruz, Cat# sc-8066, RRID: AB_2088494); anti-

DsRed (rabbit, 1:500, Clontech, Cat# 632496, RRID: AB_10013483); anti-EGFR (goat, 1:100, R&D, Cat# AF1280, RRID: AB_354717); anti-EGFR (rabbit, 1:100, abcam, Cat# 52894, RRID: AB_869579); anti-GFAP (chicken, 1:600, Millipore, Cat# PA1-10004, RRID: AB_1074620); anti-GFP (goat, 1:500, Rockland, Cat# 600-101-215, RRID: AB_218182); anti-GFP (rat, 1:500, Nacalai Tesque, Inc, Cat# 04404-84, RRID: AB_10013361); anti-GLAST (guinea pig, 1:1000, Chemicon, Cat# AB1783, RRID: AB_90949); anti-Glutamine synthetase (rabbit, 1:100, abcam, Cat# ab73593, RRID: AB_2247588); anti-Ki67 (rabbit, 1:100, abcam, Cat# ab15580, RRID: AB_443209); anti-Mash-1 (mouse, 1:100, BD Pharmingen, Cat# 556604, RRID: AB_396479); anti-MBP (rabbit, 1:100, abcam, Cat# ab40390, RRID: AB_1141521); anti-MCM2 (rabbit, 1:100, Cell signaling, Cat# 3619, RRID: AB_2142137); anti-MOG (mouse, 1:100, Millipore, Cat# MAB5680, RRID: AB_1587278); anti-Nestin (mouse, 1:100, abcam, Cat# ab105389, RRID: AB_10859398); anti-NeuN (mouse, 1:100, Millipore, Cat# 377, RRID: AB_177621); anti-Neurofilament (chicken, 1:100, abcam, Cat# ab4680, RRID: AB_304560); anti-NG2 (rabbit, 1:100, Millipore, Cat# AB5320, RRID: AB_91789); anti-Nkx2.2 (mouse, 1:100, R&D, Cat# MAB8167); anti-O4 (mouse, 1:200, Chemicon, Cat# MAB1326, RRID: AB_357617); anti-Olig2 (goat, 1:200, R&D, Cat# 2418, RRID: AB_215755); anti-Olig2 (rabbit, 1:100, Millipore, Cat# AB9610, RRID: AB_570666); anti-PDGFR β (rat, 1:50, eBioscience, Cat# 14-1402-82, RRID: AB_467493); anti-PDGFR β (goat, 1:100, R&D, Cat# AF1042, RRID: AB_2162633); anti-PDGFR α (rat, 1:100, eBioscience, Cat# 14-1401-82, RRID: AB_467491); anti-PDGFR α (goat, 1:100, R&D, Cat# AF1062, RRID: AB_2236897); anti-phospho PDGFR β (rabbit, 1:100, R&D, Cat# MAB9027); anti-Rip (mouse, 1:100, DSHB, Cat# Rip, RRID: AB_531796); anti-S100 β (rabbit, 1:200, DAKO, Cat# GA50461-2, RRID: AB_2811056); anti-serotonin (rabbit, 1:100, Immunostar, Cat# 20080, RRID: AB_572263); anti-Acetylated Tubulin (mouse, 1:1000,

Sigma, Cat# T6793, RRID: AB_477585); anti- β III Tubulin (rabbit, 1:500, Covance, Cat# MMS-435P, RRID: AB_2313773); anti- γ -tubulin (mouse, 1:200, Sigma, Cat# T6557, RRID: AB_477584). The following secondary antibodies were used: Alexa Fluor-conjugated (488, 647, 568; 1:600, Molecular probes), Cy3-conjugated (1:1000, Jackson ImmunoResearch).

ELISA

Choroid plexuses were isolated from the lateral ventricles (LVCP) and cerebrospinal fluid (CSF) extracted from the cisterna magna as described (10). 5 μ g of LVCP lysate or 10 μ l of CSF were used per replicate. Each LVCP lysate sample was prepared from 3 lateral ventricle choroid plexuses from three different mice. Each CSF sample contained CSF pooled from at least 3 different mice. ELISA analysis for PDGFAA was performed in triplicate 3 times, and for PDGFDD in triplicate 5 times, following the manufacturer's ELISA kit instructions (LsBio).

FACS

The SVZs were dissected from heterozygous hGFAP::GFP (male and female were pooled) or wild-type CD-1 mice, digested with papain 10 minutes at 37°C (Worthington, 1,200 units per 5 mice) in PIPES solution [120 mM NaCl, 5 mM KCl, 50 mM PIPES (Sigma), 0.6% glucose, 1x Antibiotic/Antimycotic (Gibco), and phenol red (Sigma) in water; pH adjusted to 7.6 and mechanically dissociated to single cells after adding ovomucoid (Worthington, 0.7 mg per 5 mice) and DNase (Worthington, 1,000 units per 5 mice). Cells were centrifuged for 10 min at 4°C without brake in 22% Percoll (Sigma) to remove myelin. We included anti-CD13 and CD31 antibodies to deplete pericytes (CD13) and endothelial cells (CD31). Cell stainings were done in 3 steps: First, cells were incubated for 20 min in anti-biotin PDGFR β (1:15, eBioscience, Cat# 13-1402-82, RRID: AB_466609), CD24-A700 (1:150, Biolegend, Cat# 101836, RRID:

AB_2566730), CD133-APC (1:300, clone 13A4, eBioscience, Cat# 17-1331-81, RRID: AB_823120), and CD13 BV45 (1:50, BD, Cat# 564354, RRID: AB_2738764) and CD31 BV45 (1:50, BD, Cat# 562939, RRID: AB_2665476) to deplete perivascular cells. Cells were washed by centrifugation at 1300 rpm for 5min. Next, cells were incubated for 10 min with Streptavidin PE-Cy7 (1:500; eBioscience), and washed by centrifugation. Finally, cells were incubated with Alexa Fluor 555- conjugated EGF for 20 min (1:100; Molecular Probes), and washed by centrifugation. All stainings and washes were carried out on ice in 1% BSA, 0.1% Glucose HBSS solution. To assess cell viability, 4',6-diamidino-2-phenylindole (DAPI; 1:1000; Sigma) was added to the cell suspension. All cell populations were isolated in a single sort using a Becton Dickinson FACS Aria II using 13 psi pressure and 100- μ m nozzle aperture and were collected in Neurosphere (NS) medium (details below). As described previously by Codega et al. (2), gates were set manually using single-color control samples, FMO controls and isotype controls. Data were analyzed with FlowJo 9.3 data analysis software and displayed using bi-exponential scaling. For each FACS experiment the cells were isolated from 5 pooled hGFAP::GFP mice.

Purified cells were collected and used for cell culture or RNA extraction for RNA-seq.

Cell Culture

Clone activation assay

To assess activation kinetics, FACS purified cells were grown in Neurosphere (NS) medium [DMEM/F12 (Life Technologies) supplemented with 0.6% Glucose (Sigma), 1x HEPES (Life Technologies), 1x Insulin-Selenium-Transferrin (Life Technologies), 1x Antibiotic/Antimycotic (Gibco), N-2 (Life Technologies) and B-27 (Life Technologies) supplements] with 20 ng/ml

EGF (Upstate) and 20 ng/ml bFGF (Sigma) and Heparin 0.7 U /ml (Sigma). Each sorted population was centrifuged after FACS for 10 min at 1300 rpm at 4°C and seeded in NS medium at a density of 1.4 cell/ μ l in 96 well plates, with at least three wells per population. For quantification of activated clones, clones were quantified at 2 days and later timepoints after plating. Clusters of two or more cells with large, bright, refractant cytoplasm were counted. Experiment was repeated 5 times.

In vitro PDGFR β blocking of FACS sorted qNSCs

For PDGFR β blocking experiments, the FACS sort strategy described above was used with anti-biotin PDGFR β (1:25; R & D Systems Cat# BAF1042, RRID: AB_2162632). After sorting, cells were plated as described for the clonal activation assay with neurosphere medium (with EGF, FGF and Heparin) in the presence of rhPDGFDD (20ng/ml; R&D) and anti-PDGFR β blocking antibody (3 μ g/ml; eBioscience /Thermo Fisher Scientific Cat# 16-1402-82, RRID: AB_469070) or with Isotype control antibody (3 μ g/ml; eBioscience/Thermo Fisher Scientific Cat# 14-4321-85, RRID: AB_470106). Clones were monitored every two days as described. Experiment was performed in triplicate 5 times.

Culture and differentiation of PDGFR β ⁺ NSCs from lateral and septal wall

GFAP::GFP⁺PDGFR β ⁺CD24⁻ cells were FACS sorted from microdissected lateral or septal walls and cultured in adherent conditions (Poly-D-lysine/ Fibronectin) for 12-14 days with lateral ventricle choroid plexus conditioned medium, which increases stem cell division (10). For differentiation, cultures were washed twice with neurosphere (NS) medium without B27 (see clone activation assay) and cultured for 2 days with FGF only. After carefully washing twice

with NS medium (without B27), cells were cultured for 4 additional days with NS medium (without B27) with 2% FCS. Cells were fixed with 4% PFA for 20 min and washed with PBS three times. Cells were stained with anti-GFAP (chicken, 1:600, Millipore, Cat# PA1-10004, RRID: AB_1074620), anti-O4 (mouse, 1:200, Chemicon, Cat# MAB1326, RRID: AB_357617) and anti- β III Tubulin (rabbit, 1:500, Covance, Cat# MMS-435P, RRID: AB_2313773) antibodies. Immunostained cultures were imaged with a Leica DMI8 system. This experiment was performed in triplicate 3 times.

Differentiation of FACS sorted populations

FACs purified populations were cultured with NS medium supplemented with EGF and FGF (20ng/ml or 10ng/ml, respectively) in adherent (Poly-D-lysine/ Fibronectin) or floating conditions. Adherent cultures or dissociated neurospheres plated on Matrigel were differentiated as described above. Differentiation was performed in triplicate 3 times.

All cell culture experiments were quantified blinded to condition.

Lysolecithin injections

2 month old male C57BL/6JRjb mice were anesthetized with isoflurane (5% for induction and 1.5% for maintenance) in O₂ and placed into a stereotaxic frame (World Precision Instruments). Focal demyelinating lesions were induced by stereotaxic injection of 1.5 ul lysolecithin solution (LPC, Sigma, 1% in 0.9% NaCl) into the corpus callosum (1 mm lateral to midline, 1.3 mm rostral to bregma, 1.7 mm deep to brain surface. 1.5 ul of saline (0.9% NaCl) was used as a control solution. Both solutions were delivered with a glass-capillary (Harvard Apparatus) mounted on a piston operated injector (Narishige) at a speed of 1ul per min. Animals recovered

in a warm chamber before being returned into their housing cages. Mice were sacrificed at different time points after lesion: 2 days post injection (dpi) or 5 dpi. n= 3 mice per group.

Image acquisition, quantification and statistical analysis

Images from immunostained sections were acquired on a LSM 700 or 800 confocal (Zeiss) using 40X and 25X objectives. For *in vivo* quantification, we used at least four sections between Bregma +1.4mm and 0mm for each animal and counted the entire septal and lateral wall in each section. For quantification of Tom⁺ Olig2⁺ cells in different domains we used sections between Bregma +1.2mm and -1mm. For quantification in the septum itself, counts were performed from the midline to a distance 30 um away from the ventricle. We quantified cells and measured the area using Fiji software (26). 4 PDGFR β ^{WT} and 4 PDGFR β ^{Δ} mice, 3 LPC and 3 saline injected mice, and 3 mice for lineage tracing were analyzed for each time point. No samples were excluded from the analysis. Analysis was performed blind to treatment whenever possible. Data are presented as average of number of cells/mm². Two-way statistical comparisons were conducted by two-tailed unpaired Student's test. Significance was established at *p<0.05, **p<0.01, ***p<0.001. In all graphs, error bars are standard error of the mean (SEM). When comparing more than two datasets, ANOVA analysis was used to determine significance followed by the Bonferroni multiple comparison test on pairwise comparisons using Prism 6 software.

For quantification of GFAP⁺ cells that express PDGFR β and the GFAP⁺EGFR⁺ population that express PDGFR β (Fig. S1L and S1M), we only counted cells in the V-SVZ. Stellate astrocytes were excluded from this quantification.

Mapping and parameter analysis of Gorditas

Gorditas were identified based on GFAP expression and tdTomato morphology. Images were acquired using an Olympus SpinSR using a 30X objective. To map the distribution of Gorditas along the rostral-caudal axis we imaged the entire medial and lateral walls of coronal sections at 6 different levels relative to Bregma (+1.25, +0.9, +0.5, -0.15, -0.55, -1.3mm) in 3 different PDGFR β ^{WT} and PDGFR β ^A mice per level. The mapped sections were aligned using the midline and the ventral tip of the corpus callosum. The maps were then projected from a coronal to a sagittal view to visualize the rostral-caudal cell distribution. Process number, soma- and nucleus-area were measured in images acquired from 3 PDGFR β ^{WT} and 3 PDGFR β ^A mice, with an Olympus SpinSR using a 60X objective. Individual z-stacks (step size 0.6 μ m) were used to identify the primary processes based on tdTomato expression and z-projections were used to measure soma area size based on tdTomato expression and nucleus area size based on DAPI staining. Astrocyte-parameter measurements were acquired from mature stellate astrocytes in the septum.

RNA-Sequencing

For RNA-sequencing experiments, RNA was isolated from FACS-sorted cells from pooled mice (three replicates per population). The experiments were performed on the following populations: hGFAP::GFP⁺ PDGFR β ⁺ CD133⁻ EGFR⁻ CD24⁻ (P β ⁺), hGFAP::GFP⁺ PDGFR β ⁺ CD133⁺ EGFR⁻ CD24⁻ (P β ⁺ CD133⁺), hGFAP::GFP⁺ PDGFR β ⁺ CD133⁺ EGFR⁺ CD24⁻ (P β ⁺ EGFR⁺) and hGFAP::GFP⁺ PDGFR β ⁻ CD133⁺ EGFR⁺ CD24⁻ (P β ⁻ EGFR⁺) from the V-SVZ, as well as hGFAP::GFP⁺ astrocytes from the cortex (CTX) with more than 500 cells per replicate per cell type. Cell populations were directly FACS-sorted into PicoPure RNA isolation kit (Arcturus) and immediately frozen on dry ice to increase RNA yield. All samples were treated with DNase

(Qiagen) during the RNA isolation step. Whole transcriptome amplification was performed using the SMARTer Ultra Low Input RNA Sequencing-HV Kit (Clontech). Sequencing libraries were generated with Nextera DNA preparation kit (Illumina) according to the HV kit's modified Nextera protocol with an input of 5 ng cDNA. Following PCR amplification, library clean-up was performed using Agencourt AMPure XP beads (Beckman Coulter). The resulting libraries were analyzed on an Agilent Bioanalyzer. High quality libraries were sequenced as paired-end 100bp reads on an Illumina HiSeq2000 or 2500 at Columbia Genome Center.

High Throughput Sequencing Data Analyses

For RNA-sequencing experiments, an average of 20+ million reads from five cell populations were aligned to the mouse reference genome sequence (mm10) using TopHat v2.1 (27) with an average alignment rate of ~80%. Prior to aligning the reads, they were quality-trimmed to remove adapter sequences and ambiguous bases using cutadapt (28) and only uniquely mapped concordant mate pairs were used in the downstream analysis. After read mapping, transcripts were assembled using Cufflinks (27) and the expression level estimation for each gene was calculated. These values are reported in fragments per kilobase of transcript per million fragments mapped (FPKM). Total read counts for each gene were calculated using HTseq (29). The differential expression analyses on the read counts were performed using EdgeR package deposited in Bioconductor (30). Adjusted p values were used to determine statistical significance.

Fig. S1.

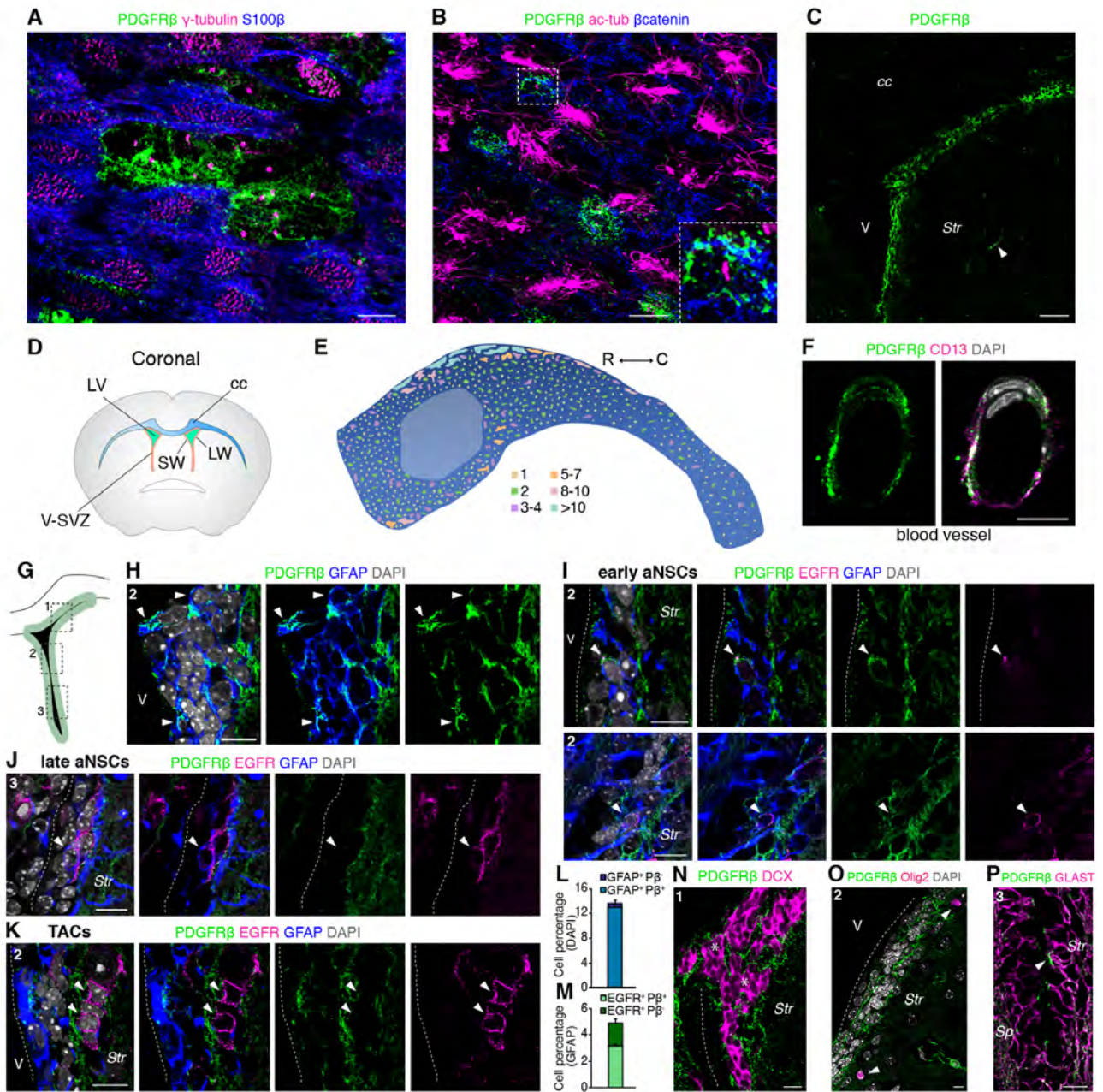


Fig. S1 Expression of PDGFR β ⁺ in the adult V-SVZ

(A) Confocal image of large cluster of PDGFR β ⁺ (green) NSCs (single basal body, γ -tubulin⁺ (magenta)) surrounded by S100 β ⁺ (blue) ependymal cells (multiple basal bodies, γ -tubulin⁺ (magenta)). (B) Confocal image of whole mount showing PDGFR β ⁺ NSCs (green) with a primary cilium labeled by acetylated tubulin (magenta). Inset shows higher magnification view of region in box. (C) Coronal section showing high levels of PDGFR β (green) in the dorsal V-SVZ. Labeled cells throughout the tissue are pericytes (arrowhead) (see S1F). (D) Coronal schema showing the lateral ventricles (LV, green), corpus callosum (cc, blue) and V-SVZ (orange) adjacent to the lateral ventricles on the lateral wall (LW) and septal wall (SW). (E) Map of lateral ventricular wall showing distribution and size of clusters of PDGFR β ⁺ NSCs. R, Rostral, C, Caudal. (F) PDGFR β (green) labels CD13⁺ pericytes (magenta) throughout the brain. (G) Coronal schema of V-SVZ with boxes and numbers indicating location of images in (H-K, N-P). (H) Coronal section showing PDGFR β expression in GFAP⁺ (blue) NSCs (arrowheads). (I) PDGFR β (green) is expressed by early aNSCs (GFAP⁺ (blue) EGFR⁺ low (magenta), arrowheads). In early aNSCs, EGFR can have different distributions. Upper panel shows focal EGFR expression and lower panel shows membrane-associated EGFR labeling. (J) PDGFR β (green) is not expressed in late aNSCs (GFAP⁺ (blue) EGFR⁺ high (magenta), arrowheads). (K) PDGFR β (green) is not expressed in transit amplifying cells (TACs) (GFAP⁻ and EGFR⁺ high, arrowheads). (L) Quantification of GFAP⁺PDGFR β ⁺ and GFAP⁺PDGFR β ⁻ cells in V-SVZ (n=4 mice). (M) Quantification of proportion of GFAP⁺ cells that are EGFR⁺PDGFR β ⁺ and EGFR⁺PDGFR β ⁻ in V-SVZ (n=4 mice). (N, O) Immunostaining of coronal sections of V-SVZ showing that (N) doublecortin⁺ (DCX, magenta) neuroblasts do not express PDGFR β (green) (asterisks), and (O) oligodendrocytes (Olig2, magenta) do not express PDGFR β (green). (P) Confocal image of V-SVZ showing that PDGFR β (green) is expressed in GLAST⁺ (magenta) cells, and that PDGFR β is enriched at the apical surface of NSCs (arrowhead). Nuclei are labeled with DAPI. V, ventricle; *Str*, striatum; *cc*, corpus callosum. Scale bars, A, B 5 μ m; C, 50 μ m; F, H, I, J, K, N, O, P 10 μ m.

Fig. S2.

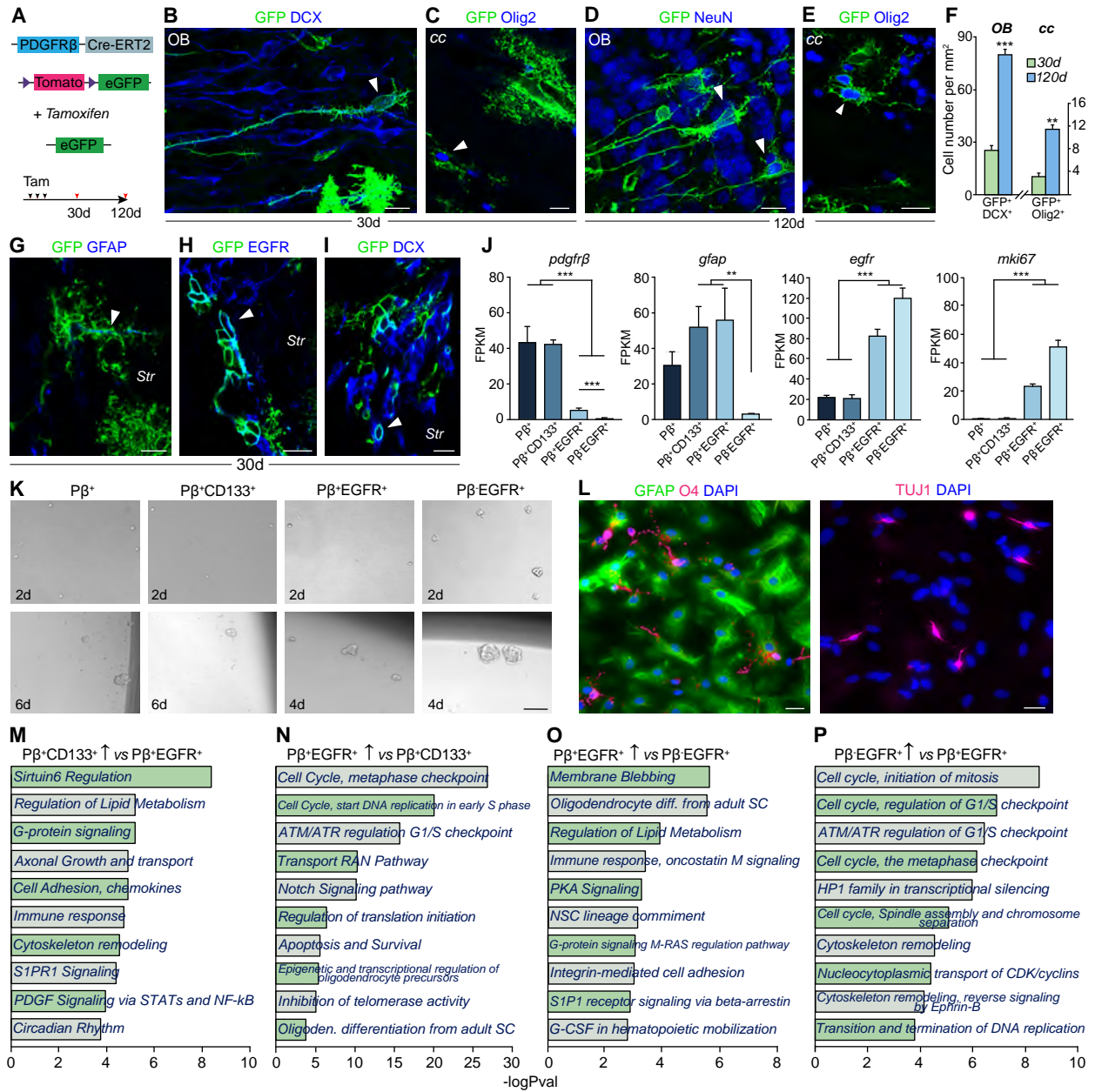


Fig. S2 Functional and molecular properties of PDGFR β ⁺ NSCs in the adult V-SVZ

(A-I) Lineage-tracing of PDGFR β ⁺ cells using PDGFR β -P2A-CreER^{T2};mT/mG mice. (A) Schema of mice and experimental paradigm. PDGFR β -P2A-CreER^{T2};mT/mG mice were injected for 3 days with tamoxifen and sacrificed 30 or 120 days later (dpi). (B, C, G-I) Images of GFP⁺ cells at 30 days and (D-E) 120 days. (B) GFP⁺DCX⁺ immature neurons in the granule cell layer of the OB at 30 dpi (arrowhead). (C) GFP⁺Olig2⁺ oligodendrocyte in the *cc* at 30 dpi (arrowhead). (D) GFP⁺NeuN⁺ mature neurons in the granule cell layer of the OB at 120 dpi (arrowheads). (E) GFP⁺Olig2⁺ oligodendrocytes in the *cc* at 120 dpi (arrowhead). In addition, GFP⁺ pericytes and stellate astrocytes were scattered throughout the brain parenchyma (data not shown) consistent with *pdgfrb* expression in these cell types (6). (F) Quantification of GFP⁺ DCX⁺ new neurons in OB and Olig2⁺ cells in the *cc*; n=4 mice. (G) GFP⁺GFAP⁺ cells with radial morphology in V-SVZ, (H) GFP⁺EGFR⁺ transit amplifying cells in V-SVZ and (I) GFP⁺DCX⁺ neuroblasts in V-SVZ at 30 dpi (arrowheads). (J) Expression of selected genes (FPKM) in purified populations. Asterisks indicate significant differential expression (fdr < 0.05). (K) Images of activated clones from FACS purified populations at different time points. (L) Images of P β ⁺CD133⁺ qNSCs differentiated into astrocytes (GFAP, green), oligodendrocytes (O4, magenta) (left panel) and neurons (TUJ1, magenta) (right panel). DAPI is in blue. (M-P) Selected top-enriched pathway maps from Metacore analysis. Comparisons of (M) P β ⁺CD133⁺ qNSCs to P β ⁺EGFR⁺, (N) P β ⁺EGFR⁺ to P β ⁺CD133⁺ qNSCs, (O) P β ⁺EGFR⁺ to P β ⁺EGFR⁺ and (P) P β ⁺EGFR⁺ to P β ⁺EGFR⁺ populations. Comparison of P β ⁺CD133⁺ qNSCs to P β ⁺EGFR⁺ highlighted known GO pathways related to quiescence (regulation of lipid metabolism, G-protein signaling, cell adhesion, and immune response) and novel (sirtuin 6 regulation, circadian rhythm, S1PR1 signaling and PDGF signaling) pathways. Pathways are ranked by $-\log(p\text{-val})$. **p<0.01, ***p<0.001. Error bars indicate SEM. *Str*, striatum; *cc*, corpus callosum; OB, olfactory bulb. Scale bars, 10 μ m.

Fig. S3.

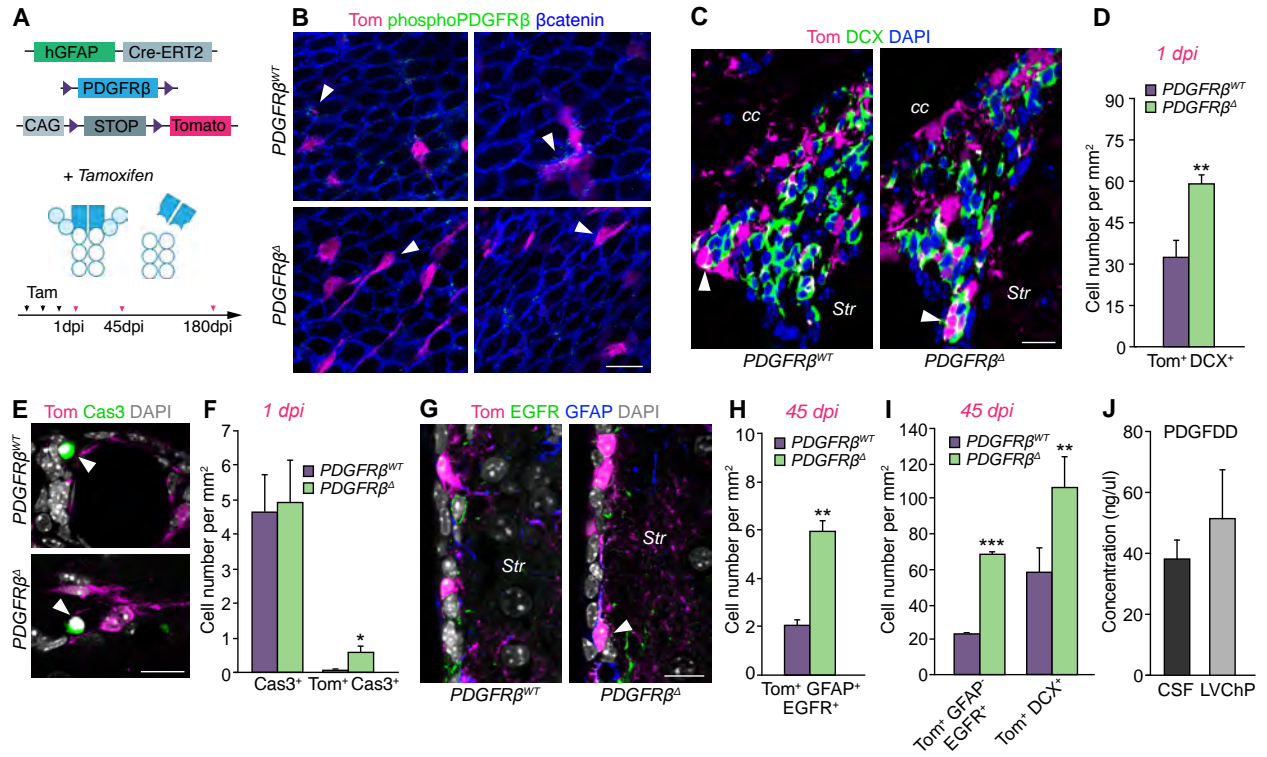


Fig. S3 PDGFR β deletion affects NSC proliferation and cell survival

(A) Schema of mouse model and experimental paradigm for inducible deletion of PDGFR β in GFAP⁺ NSCs. (B) Whole mount immunostained for Tom (magenta), phospho-PDGFR β (green) and β -catenin (blue) showing that phospho-PDGFR β is highly expressed in ventricle contacting Tom⁺ cells in PDGFR β ^{WT} mice and almost absent in PDGFR β ^{Δ} mice (arrowheads). Note high levels of phospho-PDGFR β labeling in unrecombined cells in the same whole mount from PDGFR β ^{Δ} mice (green dots). (C) Coronal sections immunostained for Tom (magenta) and DCX (green) and DAPI (blue) in V-SVZ PDGFR β ^{WT} and PDGFR β ^{Δ} mice. Arrowheads indicate Tom⁺ neuroblasts. (D) Quantification of Tom⁺ neuroblasts (Tom⁺ DCX⁺) in V-SVZ of PDGFR β ^{WT} and PDGFR β ^{Δ} mice (n=4 mice/group). (E) Images of Tom⁺ (magenta) and Caspase3⁺ (green) cells (arrowheads) in the V-SVZ of PDGFR β ^{WT} and PDGFR β ^{Δ} mice. (F) Quantification of total Caspase3⁺ and Tom⁺Caspase3⁺ cells in the V-SVZ of PDGFR β ^{WT} and PDGFR β ^{Δ} mice (n=4 mice/group). (G) V-SVZ coronal sections immunostained for Tom (magenta), EGFR (green) and GFAP (blue) at 45 dpi in PDGFR β ^{WT} vs PDGFR β ^{Δ} mice. Arrowhead indicates Tom⁺ aNSC (GFAP⁺EGFR⁺). Nuclei were stained with DAPI. (H) Quantification of aNSCs (Tom⁺GFAP⁺EGFR⁺) in PDGFR β ^{WT} vs PDGFR β ^{Δ} mice at 45dpi (n=4 mice/group). (I) Quantification of TACs (Tom⁺GFAP⁺EGFR⁺) and neuroblasts (Tom⁺DCX⁺) at 45 dpi (n=4 mice/group). (J) Concentration of PDGFDD (ng/ul) in the cerebrospinal fluid (CSF) and lateral ventricle choroid plexus (n=5 experiments). *Str*, striatum; *cc*, corpus callosum. Scale bars, 10 μ m. *p<0.05, **p<0.01, ***p<0.001. Error bars indicate SEM.

Fig. S4.

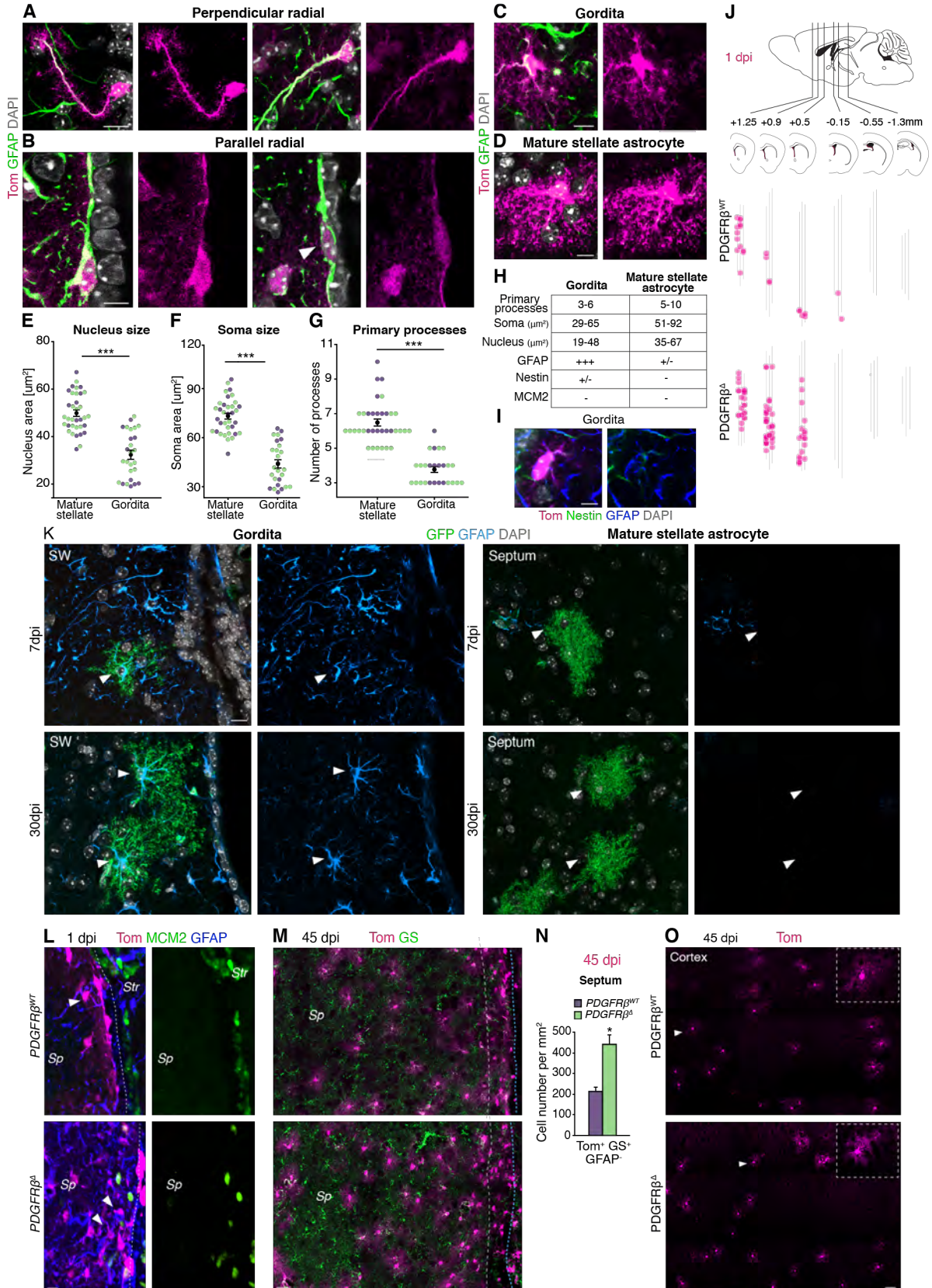


Fig. S4 GFAP⁺ cell types in the adult V-SVZ

(A-D) Confocal images showing examples of different morphologies of Tom⁺ (magenta) GFAP⁺ (green) cells at 1dpi. (A) Tom⁺GFAP⁺ radial cell perpendicular to the ventricle. (B) Tom⁺GFAP⁺ radial cell parallel to the ventricle. (C) Morphology of Tom⁺GFAP⁺ gorditas in the septal V-SVZ. (D) Tom⁺ mature stellate astrocyte. (E-I) Comparison of features of gorditas and mature stellate astrocytes (n=4 mice). (E) Quantification of nucleus area of mature stellate astrocytes and gorditas. (F) Quantification of soma area of mature stellate astrocytes and gorditas. (G) Quantification of number of primary processes in mature stellate astrocytes and gorditas. (H) Summary table comparing features of gorditas and mature stellate astrocytes. (I) Tom⁺ gordita immunostained for nestin (green) and GFAP (blue). (J) Map of distribution of gorditas in the septal/fimbria wall of the V-SVZ (also see Fig. S5D for anatomical information). Black lines represent coronal sections of 3 mice from rostral to caudal levels. Each pink dot corresponds to the location of a single gordita. (K) Lineage tracing of PDGFR β ⁺ cells in PDGFR β -P2A-CreER^{T2};mT/mG mice. Left panels show images of GFP⁺ cells with gordita morphology expressing high levels of GFAP near septal wall (SW) at 7 dpi (upper) and 30 dpi (bottom) (arrowheads). Right panels show images of GFP⁺ cells with mature stellate astrocyte morphology in septum at 7 dpi (upper) and 30 dpi (bottom) (arrowheads) with little GFAP expression. (L) Coronal section of septal wall immunostained for Tom (magenta), MCM2 (green) and GFAP (blue) in PDGFR β ^{WT} and PDGFR β ^Δ mice at 1dpi, arrowheads indicate Tom⁺ gorditas, dashed line indicates the ventricle. The majority of gorditas lack MCM2 expression. (M) Images of Tom (magenta) and Glutamine Synthetase (GS, green) immunostaining in septal V-SVZ and septum at 45 dpi in PDGFR β ^{WT} and PDGFR β ^Δ mice. Cyan dashed line on right indicates ventricle. Gorditas are found in close proximity to the V-SVZ between the ventricle and the whited dashed line, but not further away in the septum. (N) Quantification of stellate astrocytes in the septum at 45dpi in PDGFR β ^{WT} and PDGFR β ^Δ mice (n=4 mice/group). (O) Images of the cortex showing similar numbers of branched Tom⁺ astrocytes (arrowhead) in PDGFR β ^{WT} and PDGFR β ^Δ mice at 45dpi. Inset shows higher magnification. Scale bars, A, B, C, D, I 5 μ m; K, L 10 μ m; M, O, 20 μ m. *p<0.05, ***p<0.001. Error bars indicate SEM.

Fig. S5

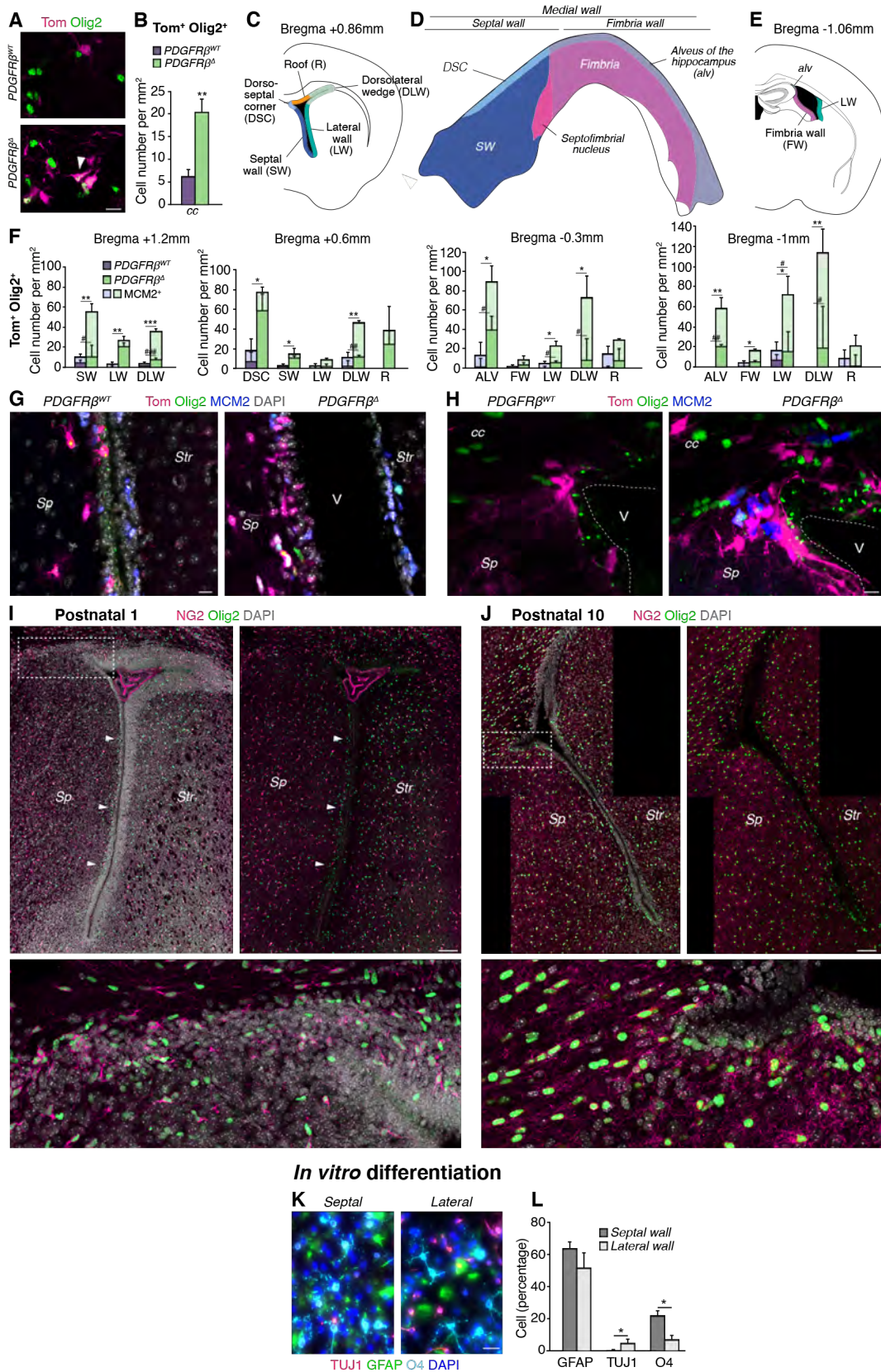


Fig. S5 Oligodendrogenic domains in the V-SVZ

(A) Confocal images of corpus callosum immunostained for Tom (magenta) and Olig2 (green) in PDGFR β^{WT} vs PDGFR β^{Δ} mice at 1dpi. (B) Quantification of Tom⁺Olig2⁺ cells in corpus callosum at 1dpi (n=4 mice/group). (C-E) Schemas showing coronal sections at Bregma +0.86mm (C) and Bregma -1.06mm (E) and names of domains analyzed in V-SVZ. (D) Schema of whole mount perspective of the entire medial wall of the lateral ventricle. In all figures, we refer to levels adjacent to the septal nuclei (blue) as the septal wall and dorsoseptal corner. At more caudal levels we refer to the fimbria (magenta) wall and alveus of the hippocampus. (F) Quantification of Tom⁺Olig2⁺ and Tom⁺Olig2⁺MCM2⁺ cells in different domains of V-SVZ in PDGFR β^{WT} and PDGFR β^{Δ} mice at Bregmas +1.2mm, +0.6mm, -0.3mm and -1.0mm (n=4 mice/group). (G) The septal wall shows an increase in Tom⁺ (magenta), Olig2⁺ (green) and MCM2⁺ cells in PDGFR β^{Δ} mice. (H) Dorsoseptal corner of V-SVZ shows an increase of Tom⁺ (magenta), Olig2⁺ (green) and MCM2⁺ cells in PDGFR β^{Δ} mice. (I, J) Upper panels show panoramic images of Olig2 (green), NG2 (magenta) immunostaining with (left) and without (right) DAPI in the V-SVZ of postnatal day 1 (I) and postnatal day 10 (J) mice. Arrowheads indicate septal wall. Lower panels show higher power view of dorsoseptal corner. (K, L) Differentiation (K) and quantification (L) of FACS-purified PDGFR $\beta^{\text{+}}$ cells from septal and lateral V-SVZ into neurons (TuJ1), astrocytes (GFAP) and oligodendrocytes (O4) (n=3 experiments). *Str*, striatum; *Sp*, septum; *cc*, corpus callosum; V, ventricle. Scale bars, A, G, H, K 10 μm ; I, J 100 μm . *p<0.05, **p<0.01, ***p<0.001, #p<0.05, ##p<0.01, ###p<0.001. Error bars indicate SEM.

Fig. S6

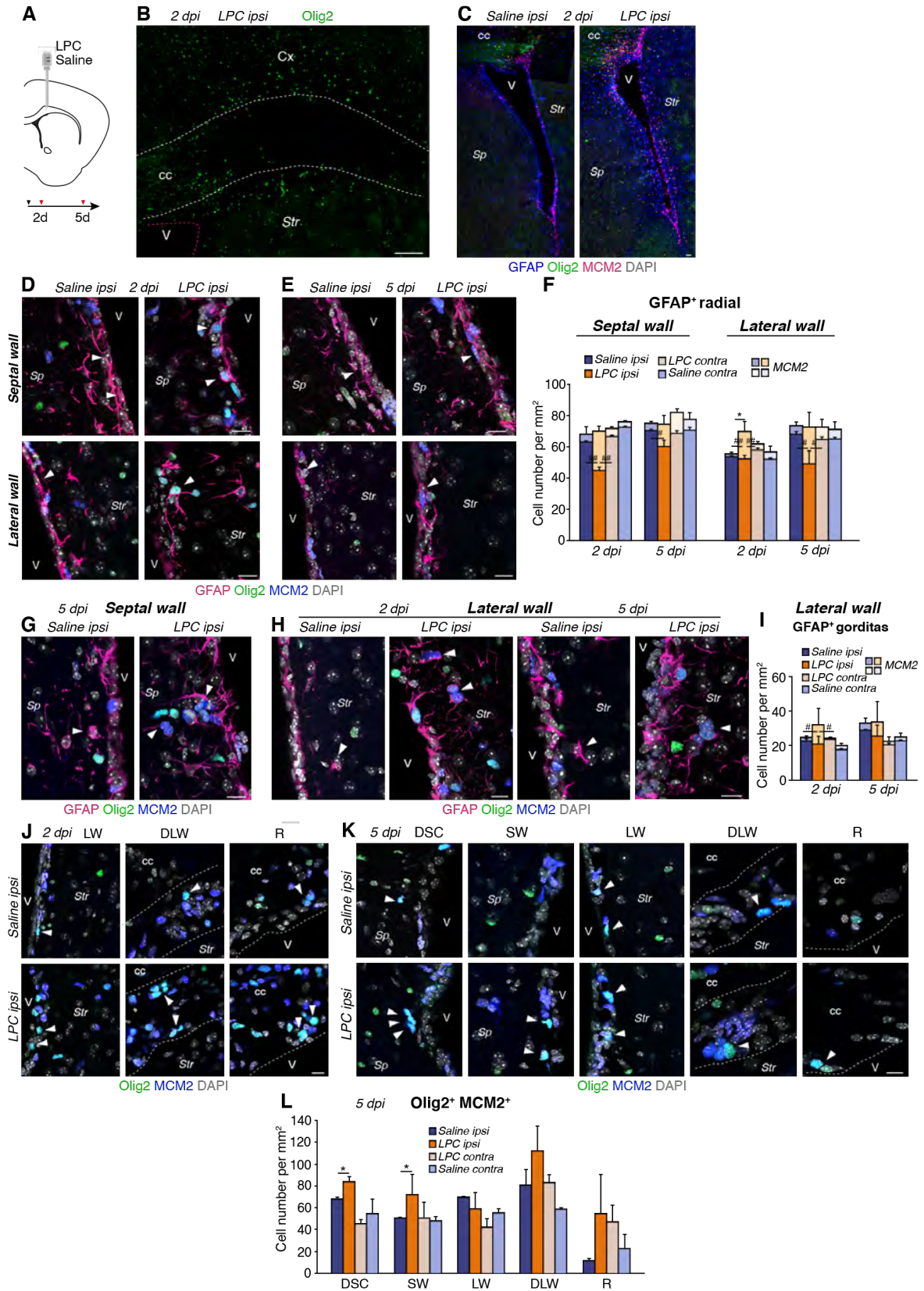


Fig. S6 Focal demyelination affects multiple domains in the V-SVZ

(A) Schema of coronal section showing location of focal demyelination in the corpus callosum. Brains were analyzed 2 or 5 days after injection of saline or lysolecithin (LPC). (B) Panoramic view of corpus callosum immunostained for Olig2 (green) showing the lack of Olig2⁺ cells in the area of demyelination at 2dpi. (C) Images of V-SVZ showing ipsilateral hemispheres of saline and LPC treated mice immunostained for MCM2 (magenta), Olig2 (green) and GFAP (blue). (D-F) Radial stem cell response to focal demyelination. (D) Images of septal wall (upper) and lateral wall (bottom) immunostained for GFAP (magenta), Olig2 (green), MCM2 (blue) of saline and LPC treated mice at 2 dpi. White arrowheads indicate radial cells. (E) Images of septal wall (upper) and lateral wall (bottom) immunostained for GFAP (magenta), Olig2 (green) and MCM2 (blue) of saline and LPC treated mice at 5 dpi. White arrowheads indicate radial cells. (F) Quantification of GFAP⁺ radial and proliferating radial cells in the septal wall and lateral wall at 2 dpi and 5dpi (n=3 mice/group). (G-I) Gorditas response to focal demyelination. (G) Images of GFAP (magenta), Olig2 (green) and MCM2 (blue) immunostaining in septal wall at 5 dpi, arrowheads indicate gorditas. (H) Images of GFAP (magenta), Olig2 (green) and MCM2 (blue) immunostaining in lateral wall at 2 and 5 dpi, arrowheads indicate gorditas. (I) Quantification of GFAP⁺ gorditas and proliferating (MCM2) gorditas in the lateral wall at 2 and 5 dpi (n=3 mice/group). (J) Images of Olig2 (green), MCM2 (blue) and DAPI immunostaining in different V-SVZ domains of saline and LPC treated mice at 2 dpi, white arrowheads indicate MCM2⁺ and Olig2⁺ cells. (K) Images of Olig2 (green), MCM2 (blue) and DAPI immunostaining in different V-SVZ domains of saline and LPC treated mice at 5 dpi, white arrowheads indicate MCM2⁺ and Olig2⁺ cells. (L) Quantification of Olig2⁺ MCM2⁺ cells in different V-SVZ domains of saline and LPC treated mice at 5dpi (n=3 mice/group). LW, lateral wall; SW, septal wall; DSC, dorsoseptal corner; DLW, dorsolateral wedge; R, roof; *Sp*, septum; *Str*, striatum; *cc*, corpus callosum; V, ventricle. Scale bars, D, E, G, H, J, K, 10μm; C 20μm; B 100μm. *p<0.05, #p<0.05, ##p<0.01. Error bars indicate SEM.

Fig. S7.

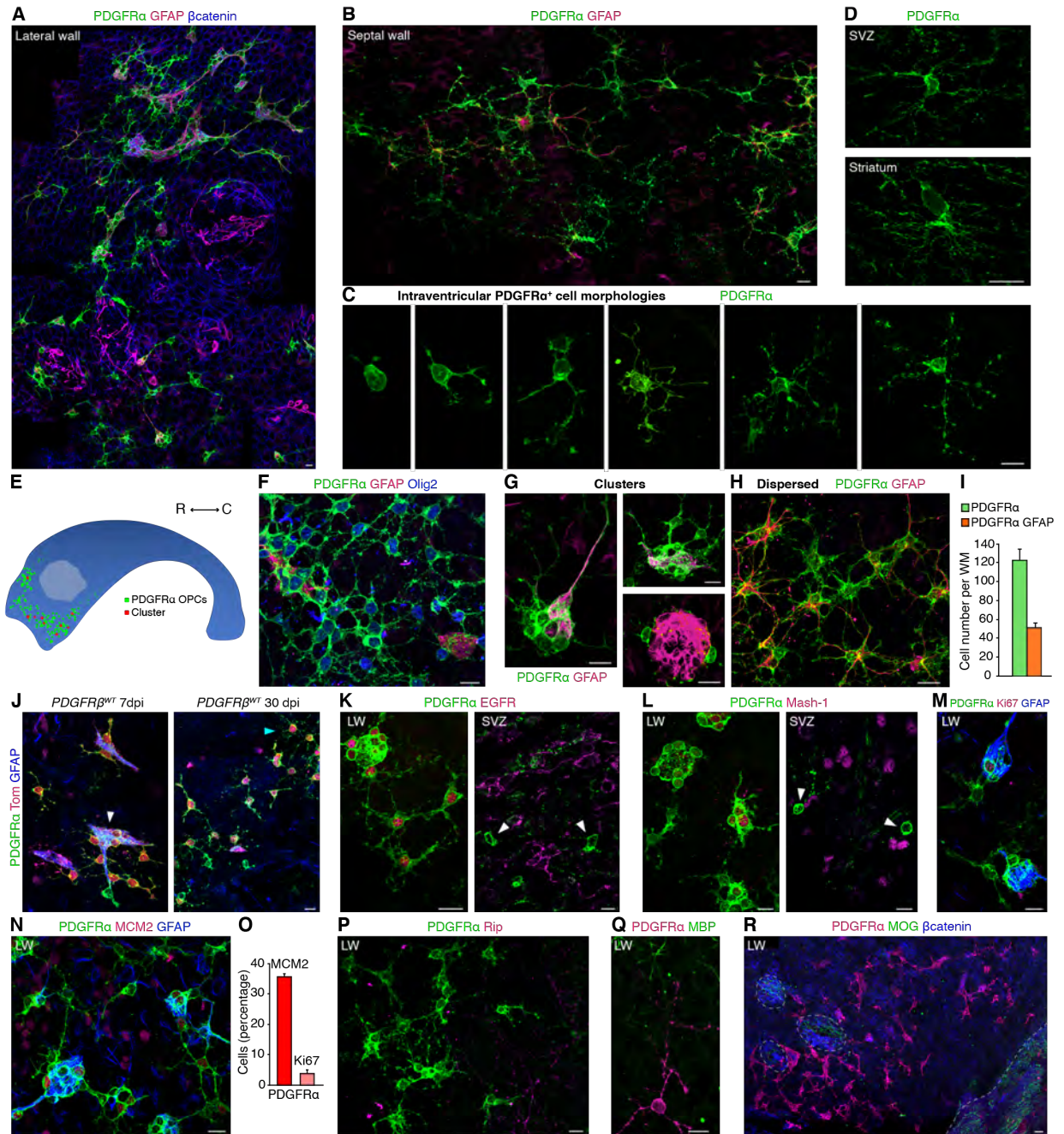


Fig. S7 Characterization of intraventricular OPCs

(A) Low power view of rostral area of whole mount of lateral wall immunostained for PDGFR α (green), GFAP (magenta) and β -catenin (blue) showing the distribution of intraventricular PDGFR α ⁺ OPCs. (B) Whole mount of septal wall immunostained for PDGFR α (green), and GFAP (magenta) showing intraventricular PDGFR α ⁺ OPCs on the septal wall. (C) Collage showing different morphologies of intraventricular PDGFR α ⁺ OPCs from less to more mature. (D) Images showing morphology of parenchymal PDGFR α ⁺ cells deeper in the SVZ and in the striatum. (E) Distribution of intraventricular OPCs and clusters with GFAP⁺ cells. (F) Whole mount immunostaining showing PDGFR α ⁺ (green) OPCs express Olig2 (blue). (G) Whole mount immunostaining showing examples of PDGFR α ⁺ GFAP⁺ clusters and (H) examples of dispersed PDGFR α ⁺ and PDGFR α ⁺ GFAP⁺ cells. Once dispersed, many maintain contact with each other. (I) Quantification of PDGFR α ⁺ only and PDGFR α ⁺ GFAP⁺ cells per whole mount (n=4 mice). (J) Lineage tracing of Tom⁺ OPCs in PDGFR β ^{WT} mice at 7dpi and 30dpi. At 7dpi, many cells are found in GFAP⁺/PDGFR α ⁺ clusters (white arrowhead). At 30dpi (right) Tom⁺ PDGFR α ⁺ cells have a more mature branched morphology (blue arrowhead). (K) Whole mount immunostained for PDGFR α (green) and EGFR (magenta) showing that most intraventricular PDGFR α OPCs expressed EGFR in the nucleus (left), whereas PDGFR α ⁺ OPCs in the SVZ do not express EGFR (right). (L) Confocal image of whole mount showing that most intraventricular PDGFR α ⁺ (green) OPCs are Mash1⁺ (magenta, left) but PDGFR α ⁺ OPCs in the SVZ are not (right, arrowhead). (M) Image showing that some intraventricular PDGFR α ⁺ (green) OPCs are Ki67⁺ (magenta) in the cluster. (N) Whole mount immunostained for PDGFR α (green), GFAP (blue) and MCM2 (magenta) showing proliferating intraventricular PDGFR α OPCs in clusters and dispersed PDGFR α OPCs. (O) Quantification of intraventricular PDGFR α ⁺ MCM2⁺ and PDGFR α ⁺ Ki67⁺ OPCs (n=3 mice). (P) Images of whole mount immunostaining for PDGFR α (green) and Rip (magenta) showing that PDGFR α ⁺ OPCs are not myelinated. Visible Rip⁺ processes (magenta) are deeper in the SVZ. (Q) Whole mount immunostained with PDGFR α (magenta) and myelin basic protein (MBP) (green) showing that PDGFR α ⁺ OPCs do not express MBP. (R) Panoramic view of whole mount immunostained with PDGFR α (magenta), MOG (green) and β catenin (blue) showing that myelinating cells are not present on the surface of the wall, in contrast to the commissure (to right of dashed line). Dashed circles show myelinated axons in the striatum where the wholemount was nicked during preparation,

damaging the ependymal layer. Scale bars, 10um.

Fig. S8.

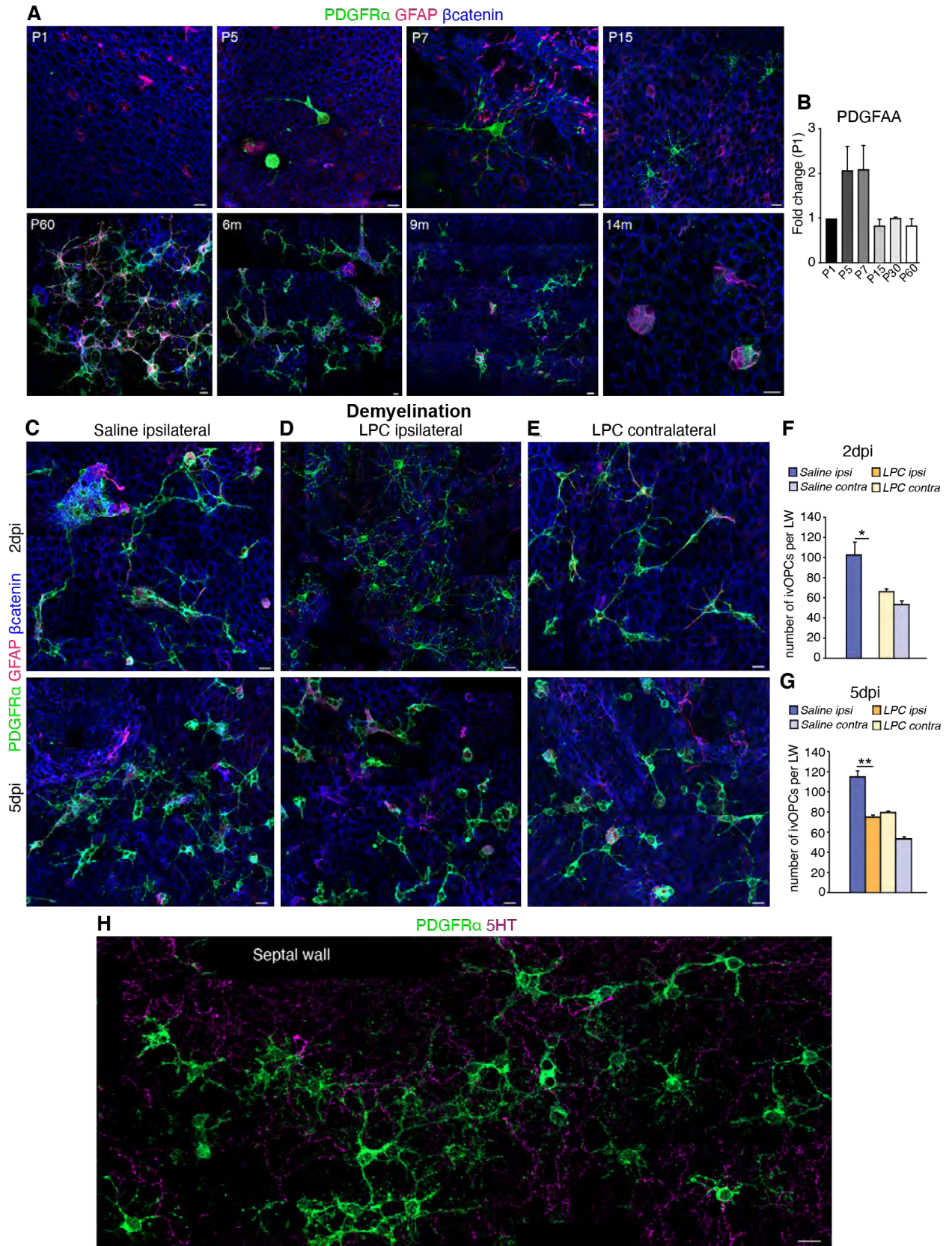


Fig. S8 Intraventricular OPC appearance during development and response to demyelination

(A) Whole mounts immunostained for PDGFR α (green), GFAP (magenta) and β -catenin (blue) showing the distribution of intraventricular PDGFR α ⁺ OPCs in the lateral V-SVZ from postnatal day 1 to 14 month old mice. Intraventricular PDGFR α ⁺ OPCs appear for the first time at Postnatal 5 (P5). With increasing age, more clusters are found, and fewer dispersed OPCs. (B) Concentration of PDGFAA ligand in the choroid plexus of the lateral ventricles during postnatal development as measured by ELISA (n=3 experiments). (C-G) Demyelination. (C-E) Confocal images of whole mount immunostained for PDGFR α (green), GFAP (magenta) β -catenin (blue) showing intraventricular OPCs of (C) saline ipsilateral wall at 2 dpi (top) and 5 dpi (bottom); (D) LPC ipsilateral wall at 2 dpi (top) and 5 dpi (bottom). At 2dpi, only parenchymal OPCs are present on the LPC ipsilateral side. (E) LPC contralateral wall at 2 dpi (top) and 5 dpi (bottom). (F) Quantification of intraventricular PDGFR α ⁺ OPCs per lateral wall whole mount in saline and LPC treated mice at 2 dpi (n=3 mice/group). (G) Quantification of intraventricular PDGFR α ⁺ OPCs per lateral wall whole mount in saline and LPC treated mice at 5 dpi (n=3 mice/group). (H) Confocal image of PDGFR α (green) and Serotonin (5HT) (magenta) showing that intraventricular PDGFR α ⁺ OPCs contact supraependymal serotonergic axons on the septal V-SVZ. Scale bars, 10um. *p<0.05, **p<0.01. Error bars indicate SEM.

Additional Data Supplementary Tables

Table S1. RNA seq. List of expression values in FPKM (fragments per kilobase of transcript per million mapped reads) from 5 FACS purified populations (three replicates per population).

Table S2. RNA seq. List of differentially expressed genes across PDGFR β^+ qNSCs, PDGFR β^+ EGFR $^+$ and PDGFR β^- EGFR $^+$ population comparisons.

Table S3. Top enriched pathway maps from Metacore analysis comparing PDGFR β^+ qNSCs, PDGFR β^+ EGFR $^+$ and PDGFR β^- EGFR $^+$ populations.